Communication of IUGS Geological Standards

121

by Maria Marino[1], Patrizia Maiorano[1], Angela Girone[1], Salvatore Gallicchio[1], Franck Bassinot[2], Sebastien Nomade[2], Quentin Simon[3], Adele Bertini[4], Timothy Herbert[5], Paola Petrosino[6], Marina Addante[1], Rafael La Perna[1], Samanta Trotta[1], and Neri Ciaranfi[1]*

The Ideale section at Montalbano Jonico (southern Italy): a Standard Auxiliary Boundary Stratotype (SABS) for the Middle Pleistocene Subseries of the Quaternary System

[1] Dipartimento di Scienze della Terra e Geoambientali, Università degli Studi di Bari Aldo Moro, via E. Orabona 4, 70125 Bari, Italy; *Corresponding author: E-mail: maria.marino@uniba.it
[2] Laboratoire des Sciences du Climat et de L'Environnement, UMR8212, LSCE/IPSL, CEA-CNRS-UVSQ and Université Paris-Saclay, Gif-Sur-Yvette, France
[3] Aix Marseille Univ, CNRS, IRD, INRAE, Coll France, CEREGE UM 34, Aix en Provence, 13545, France. Walloon High Strategic Council, Place Joséphine-Charlotte 2, 5100, Namur, Belgium
[4] Dipartimento di Scienze della Terra, Università degli Studi di Firenze, via G. La Pira 4, 50121, Firenze, Italy
[5] Department of Earth, Environmental, and Planetary Sciences, Institute at Brown for Environment & Society, Brown University, Providence, RI, USA
[6] Dipartimento di Scienze della Terra dell'Ambiente e delle Risorse, Università degli Studi di Napoli Federico II, Largo San Marcellino 10, 80138, Napoli, Italy

(Received: July 31, 2023; Revised accepted: September 15, 2023)

https://doi.org/10.18814/epiiugs/2023/023022

The Ideale section (IS) at Montalbano Jonico, Italy, has been approved as a Standard Auxiliary Boundary Stratotype (SABS) for the Global boundary Stratotype Section and Point (GSSP) of the Middle Pleistocene Subseries/Subepoch and Chibanian Stage/Age at the Chiba section, Japan. The proposal was submitted to the voting members of the International Commission on Stratigraphy's Subcommission on Quaternary Stratigraphy (SQS) on May 4, 2023, and following discussions was approved on July 8, 2023. The 74 m thick IS continuously spans the Marine Isotope Stage (MIS) 20–18 interval, and is part of the longer Montalbano Jonico succession (Basilicata, southern Italy in the Mediterranean region) encompassing MIS 37 to early MIS 16. The IS provides a detailed record based on multiple chronologically well constrained marine and terrestrial proxies, which are particularly useful for outlining the paleoclimatic evolution through the Lower–Middle Pleistocene transition. The high-resolution carbon and oxygen isotope stratigraphy outlines glacial–interglacial and stadial–interstadial phases as well as the sub-millennial-scale features of Termination IX and the onset of MIS 19c. The sapropel layer equivalent to insolation cycle 74 (784 ka) occurs in early MIS 19c. A prominent peak in the $^{10}Be/^{9}Be$ record at the MIS 19c–19b transition identifies the low geomagnetic dipole moment associated with the Matuyama–Brunhes boundary interval. Two tephra layers (V3 and V4) relevant to boundary interval are $^{40}Ar/^{39}Ar$ dated. The V4 layer, occurring at the MIS 19c–b transition and in the middle of the $^{10}Be/^{9}Be$ peak, has an age of 774.1±0.9 ka, corresponding to the age of the Middle Pleistocene GSSP. A high-resolution alkenone sea-surface temperature and several paleobiological records complement the rich chronological and paleoenvironmental dataset from MIS 20 to the inception of MIS 18. The GSSP boundary interval in the IS is represented from 35.50 to 39.50 m, which corresponds to the interval of the highest values of the $^{10}Be/^{9}Be$ ratio (~776.35–771.87 ka) and includes the V4 tephra layer and the MIS 19c–MIS 19b transition. This SABS extends the correlation potential of the Middle Pleistocene Subseries/Subepoch GSSP interval to the Mediterranean region.

Introduction

The Subcommission on Quaternary Stratigraphy (SQS) of the International Commission on Stratigraphy (ICS) in 2002 established a Working Group to examine all aspects of the proposed Early–Middle Pleistocene boundary including the criteria to be followed in selecting the Global boundary Stratotype Section and Point (GSSP). At the 32nd International Geological Congress in Florence in 2004, this working group recommended that the boundary be defined in a marine section at a point "close to" the Matuyama–Brunhes palaeo-

magnetic reversal (MBB) (Head et al., 2008), following suggestions that had arisen from XIIth INQUA Congress in Ottawa in 1987 (Richmond, 1996; Head et al., 2008). At the Florence congress, three potential candidates for the GSSP were presented: Chiba in Japan, Montalbano Jonico in Basilicata, and Valle di Manche in Calabria, the last two being in Italy. After visiting all three sites during the workshop in Italy (Ciaranfi et al., 2015) and in Japan (Okada and Suganuma, 2018), the SQS Working Group inspected the proposals of the three final candidates from July to November 2017, and voted, by supermajority, for the Chiba composite section (CcS). This was followed in 2018 by voting within the SQS which further recommended the Chiba proposal, and the ICS approved the proposal in 2019. The Executive Committee of the International Union of Geological Sciences (IUGS) ratified the GSSP for the base of the Chibanian Stage/Age and Middle Pleistocene Subseries/Subepoch at the Chiba section of the Chiba composite section on January 17, 2020 (Head, 2021; Head et al., 2021). The final GSSP proposal was published by Suganuma et al. (2021). The CcS was considered the best section to host the GSSP primarily because it contains a robust record of the MBB. This paleomagnetic boundary is recorded at the CcS by a flip of the virtual geomagnetic pole (VGP- latitudes) and a drop in the geomagnetic field intensity based on both the paleomagnetic record and on the authigenic $^{10}Be/^{9}Be$ ratio data (Suganuma et al., 2015, 2021; Okada et al., 2017; Simon et al., 2019; Haneda et al., 2020a). The GSSP of the Chibanian Stage is positioned 1.1 m below the directional midpoint of the MBB (astronomical age 772.9 ka), at the base of the Ontake-Byakubi-E tephra bed (Byk-E, U-Pb zircon age of 772.7 ± 7.2 ka, astronomical age of 774.1 ka, Suganuma et al., 2021).

A crucial step in making a GSSP more useful is to extend its correlation potential at global scale. The ICS has recently approved the use of the Standard Auxiliary Boundary Stratotype (SABS), which is a section designated to represent a detailed complementary expression of the boundary interval, aiming to assist in the correlation of a GSSP between continents, biogeographic provinces, climatic zones and depositional facies (Head et al., 2023a, b). Such a goal serves the scientific community well and is particularly meaningful for the Chibanian Stage GSSP because the Lower Pleistocene GSSPs for the Gelasian (Rio et al., 1998; Gibbard et al., 2010) and Calabrian (Aguirre and Pasini, 1985; Cita et al., 2008, 2012; Head, 2019) stages are located far from Japan while being stratigraphically well represented in sedimentary successions of the Mediterranean area (Capraro and Maiorano, 2023; https://stratigraphy.org/gssps/#quaternary).

The Ideale section (IS), cropping out in southern Italy, represents part of the longer Montalbano Jonico marine sedimentary succession that covers Marine Isotope Stage (MIS) 37 to early MIS 16. On July 8, 2023, the IS has been positively considered by SQS voting members as a SABS of the Chibanian Stage GSSP in Japan by virtue of its high correlation potential based on an extensive chronological, stratigraphic, paleoenvironmental and paleoclimate dataset embracing MIS 20 to early MIS 18 (Ciaranfi et al., 2010; Maiorano et al., 2016; Simon et al., 2017; Nomade et al., 2019).

The SABS proposal was submitted to the voting members of the SQS on May 4, 2023, and following discussions was approved by this subcommission on July 8, 2023 with the following results: 18 in favour, 0 against, no abstentions; with 21 eligible.

Geological Setting

The Montalbano Jonico succession (MJS) crops out at the south-western margin of the Bradanic Trough about 16 km inland from the Ionian Coast (Fig. 1A). The Bradanic Trough (e.g., Casnedi, 1988), located between the Apennines Chain to the west and the Apulian foreland to the east (Fig. 1A), is considered a post-Messinian Apennines foredeep basin (Patacca and Scandone, 2007, and references therein). The foredeep was characterized by high rates of subsidence until the Calabrian, when it underwent diachronous uplift starting from the north-west (Genzano-Banzi area) during the late Calabrian and proceeding south-eastwards to the present Ionian coast until the Holocene. In the late Calabrian, the central sector of the Bradanic Trough emerged, while the southern sector, where the Montalbano Jonico section is located, was still, reaching maximum deepening in the Early–Middle Pleistocene (e.g., Maiorano et al., 2016). From the Middle Pleistocene, sedimentation underwent a shoaling-upwards trend due to uplift of the area (uplift rate of 0.1–0.8 mm/years, Doglioni et al., 1996; Westaway and Bridgland, 2009) until its emergence.

The Montalbano Jonico clayey succession belongs to the argille subapennine informal unit (Azzaroli et al., 1968), representing its middle–upper portion. It stratigraphically overlies the allochthonous units of the chain and locally rests on Pliocene sandy units of coastal facies (sands and conglomerates of Serra del Cavallo, Mostardini and Pieri, 1967), and unconformably passes upwards into Middle–Upper Pleistocene terraced sands and conglomerates of transitional and continental environments (e.g., Pieri et al., 1996).

A large-scale geological map of the Special Natural Reserve of the Montalbano Jonico badlands represents in detail the geometry and spatial relationships between the main stratigraphical and structural features of the Montalbano Jonico composite section (Gallicchio et al., 2023). The argille subappennine unit outcrops widely in this area, mainly as badlands (Fig. 1B), showing a broad monocline gently dipping towards the eastern quadrants. This clayey monocline is better highlighted by the presence of several tephra layers and appears slightly displaced by few normal faults. The sandy and conglomerate marine terraced deposits belong to two distinct orders and unconformably overlie the argille subappennine respectively at about 290–280 m a.s.l. (MIS 13?) and at about 255–224 m a.s.l. (MIS 11? Gallicchio et al., 2023). Inland of the Ionian coast, the marine and fluvial terrace deposits are represented by distinctive regressive coastal wedges and alluvial plains at decreasing heights and ages from the hinterland (maximum height at 450 m a.s.l.) towards the present shoreline (minimum height at about 12 m a.s.l.). They testify to the gradual emergence of the Bradanic Trough and its interaction with Quaternary glacio-eustatic sea-level changes from MIS 17 (?) to MIS 5 (e.g., Cilumbriello et al., 2008; Westaway and Bridgland, 2009; Tropeano et al., 2013; Boenzi et al., 2014).

Hydrological and Atmospheric Context

Sediments of the MJS were deposited in the paleo-Gulf of Taranto (Fig. 1A), in the northern Ionian Sea, an area sensitive to short-term climate variability even in the last few millennia (e.g., Grauel et al.,

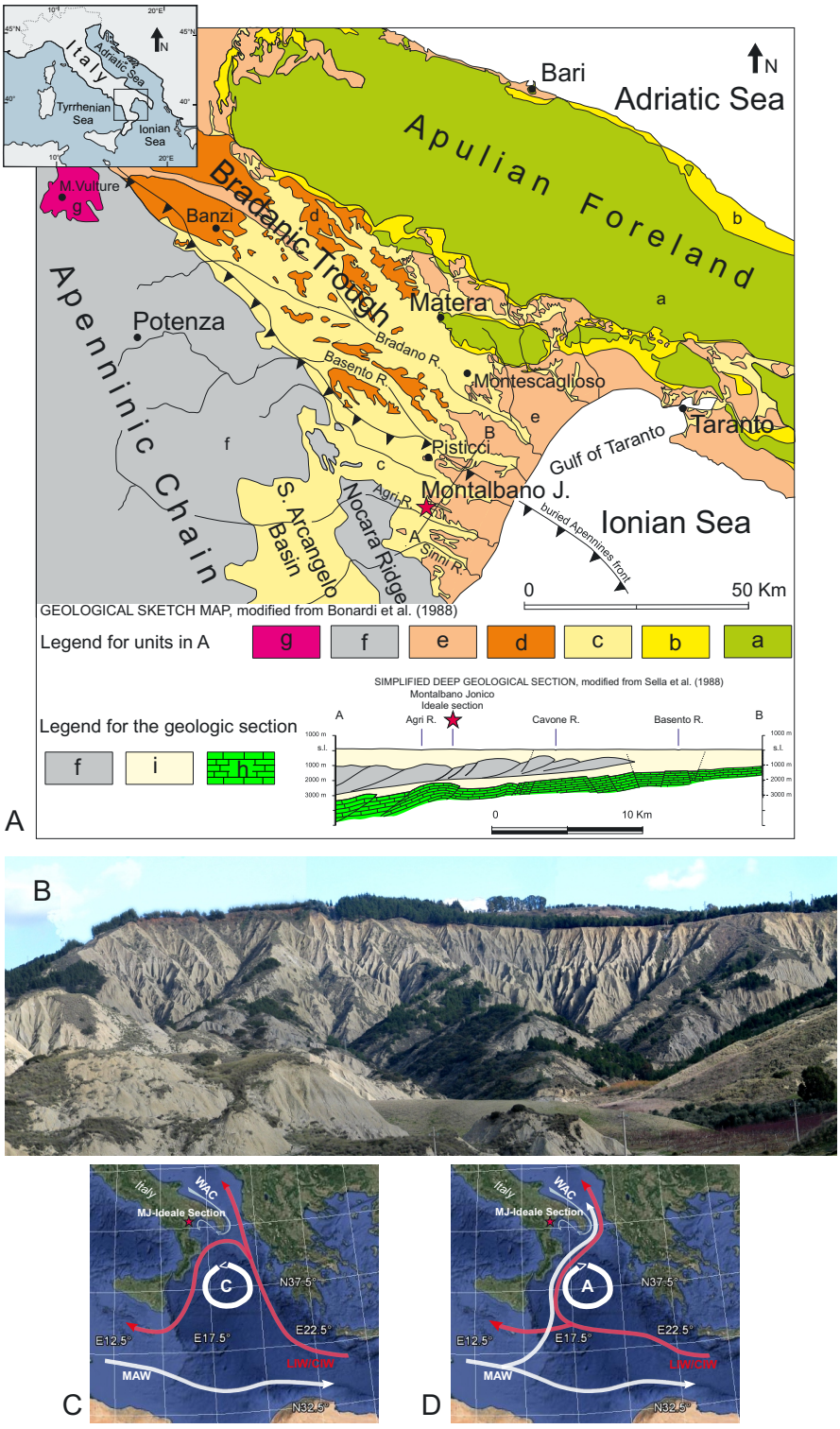

Figure 1. A: Simplified regional geological setting of southern Italy. The location of the Montalbano Jonico section is indicated by the red star. Legend of the geological map in figure A: a) Cretaceous calcareous units of the Apulian Foreland; b) Calcareous units of the Plio–Pleistocene Apennines Foredeep; c) Siliciclastic units of the Plio–Pleistocene Apennines Foredeep; d) Lower Pleistocene regressive conglomerates of the Bradanic Trough; e) Middle–Upper Pleistocene marine terraced deposits of the Bradanic Trough; f) Triassic–Neogene units of the Apennines Chain; g) Quaternary volcanic units. Legend of the geological section: h) Mesozoic–Cenozoic calcareous units of the Apulia Foreland and Apennines Foredeep (this unit includes units a and b in the map); i) Plio–Quaternary siliciclastic units of the Apennines Foredeep (this unit includes units c and e in the map); f) Triassic–Neogene units of the Apennines Chain. B: panoramic view of Montalbano Jonico badlands. C and D: main sea surface and subsurface water currents and decadal-scale cyclonic (C) and anticyclonic (D) circulation in the Ionian Sea, redrawn from Gačić et al. (2010). MAW: modified Atlantic water; LIW/CIW: Levantine/Cretan intermediate waters; WAC: Western Adriatic current.

2013; Taricco et al., 2015). In the modern Gulf of Taranto, especially in its western part, detrital sediment supply mainly comes from Apennines rivers (Goudeau et al., 2013). Sediments from the North Adriatic are also provided by the Western Adriatic Current (WAC) (Fig. 1C–D), which flows in a narrow coastal zone from the northern Adriatic Sea into the Gulf of Taranto (Poulain, 2001; Bignami et al., 2007; Turchetto et al., 2007). The low-salinity nutrient-rich coastal WAC is characterized by significant inter-annual variability (Milligan and Cattaneo, 2007) and has a greater influence in winter and spring (Poulain, 2001). The WAC mixes with the warmer and more saline Ionian Surface Water, which enters the Gulf of Taranto from the central Ionian Sea. Surface water circulation is also influenced by Modified Atlantic Water, which enters the Ionian Sea in variable mode depending on action of the Northern Ionian Gyre (NIG). In the Gulf of Taranto, the highly saline Levantine Intermediate Water (LIW), flowing from the central Ionian Sea, may be recorded at water depths of 200-600 m (Savini and Corselli, 2010). The NIG has decadal-scale cyclonic and anticyclonic phases (Civitarese et al., 2010). The cyclonic phase is characterized by saltier Levantine/Cretan Intermediate Waters (LIW/CIW) that flow northwards into the Adriatic (Fig. 1C), while the anticyclonic phase records advection of less saline Ionian water diluted by Modified Atlantic Waters (MAW) (Fig. 1D) (Civitarese et al., 2010). The alternating anticyclonic and cyclonic states are known as the Adriatic-Ionian bimodal oscillation system (Civitarese et al., 2010; Gačić et al., 2010) and they may influence nutrient distribution, water column structure and salinity, upwelling phenomena and phytoplankton growth (Civitarese et al., 2010; Batistić et al., 2017).

The present-day Mediterranean climate is characterized by warm, dry summers and cool, wet winters, as a result of seasonal shifts of the subtropical high-pressure belt and the mid-latitude westerly system (Lionello et al., 2006; Lionello, 2012). Winter precipitation is promoted by the southernmost location of the subtropical high, which brings rainy westerlies from the Atlantic Ocean over the Mediterranean. A prevailing anti-cyclonic atmospheric circulation over the Mediterranean favors summer dryness associated with the northwards displacement of the Hadley cell and of the Intertropical Convergence Zone (ITCZ). The current Mediterranean trophic regime is one of the world's poorest (Bethoux et al., 1998) and has a seasonal dynamic linked to late fall-winter mixing and summer stratification, and to nutrient supply from deep waters or from onland and atmospheric sources (D'Ortenzio & Ribera d'Alcalà, 2009; Civitarrese et al., 2010).

The Montalbano Jonico Composite Section

The Montalbano Jonico composite section (MJS), about 450 m thick, consists of a coarsening-upwards sedimentary succession ranging from silty clays to silty sands and includes nine tephra layers (V1–V9) (Fig. 2). The tephra layers are chemically and mineralogically distinctive and have been correlated with analogous layers in south-central Italy lacustrine and marine successions, within a Lower–Middle Pleistocene Mediterranean tephrostratigraphic framework (Petrosino et al., 2015). The V3, V4 and V5 layers have been radiometrically dated and their $^{40}Ar/^{39}Ar$ ages are 801.2 ± 19.5 ka for V3 (Maiorano et al., 2010), 773.9 ± 1.3 ka (Petrosino et al., 2015) and 774.1 ± 0.9 ka (Nomade et al., 2019) for V4, and 719.5 ± 12.6 ka (Ciaranfi et al., 2010) for V5. The V5 layer has been successfully re-dated at the Laboratoire des Sciences du Climat et de l'Environnement (LSCE, Gif Sur Yvette, France). The $^{40}Ar/^{39}Ar$ age obtained is 716 ± 1.0 ka (2s), which improves the precision of this chronological tie-point. In the supplementary materials (S1–S3) a figure (S1), the analytical protocol (S2) as well as the full dataset (S3) regarding this new age can be found. V5 is an important regional marker found in numerous records including the lacustrine Ohrid ("tephra OH-DP-2699", Wagner et al., 2019) and Sulmona ("tephra SUL2-1", Giaccio et al., 2013) sections, and marine Valle di Manche section ("Parmenide ash", Capraro et al., 2005, 2011). Therefore, the V5 age can be used to synchronize the chronology of these sedimentary records.

Table 1. Numerical ages of calcareous plankton bioevents in the Montalbano Jonico composite section, including end temporary disappearance of G. omega at the Ideale section, according to Ciaranfi et al. (2010), Maiorano et al. (2010) and Nomade et al. (2019)

Calcareous Plankton Biochronology					
Montalbano Composite Section				Additional calibrated ages (Ma)	
Bioevent	Depth (m)	Age (Ma)	MIS	Atlantic/Pacific	Mediterranean
end temp. disap. *Gephyrocapsa omega*	53.5 Ideale partial section	0.766	19a-2	0.78*	0.78*
beginning temp. disap. *Gephyrocapsa omega*	82.65 Interval B	0.83	21-20	0.82*	0.82*
HCO *Reticulofenestra asanoi*	162.85 Interval A	0.92	23	0.91**	0.90**
LO *G. omega* (= re-entrance medium *Gephyrocapsa*)	138.15 Interval A	0.96	25	1.01** Atl. 1.04** Pac.	0.96**
LCO *Reticulofenestra asanoi*	70.95 Interval A	1.09	31	1.14**	1.08**
end influx *Globorotalia crassaformis*	60.55 Interval A	1.12	34-33	.	1.12***
beginning influx *Globorotalia crassaformis*	50.15 Interval A	1.15	34	.	1.15***
re-appearance *Neogloboquadrina pachyderma* sinistral	17.2 Interval A	1.21	36	.	1.21***

Calibrations from reference records are reported. *Maiorano et al. (2010); **Lourens et al. (2004); ***Lirer et al. (2019). LO: Lowest Occurrence; LCO: Lowest Common Occurrence; HCO: Highest Common Occurrence

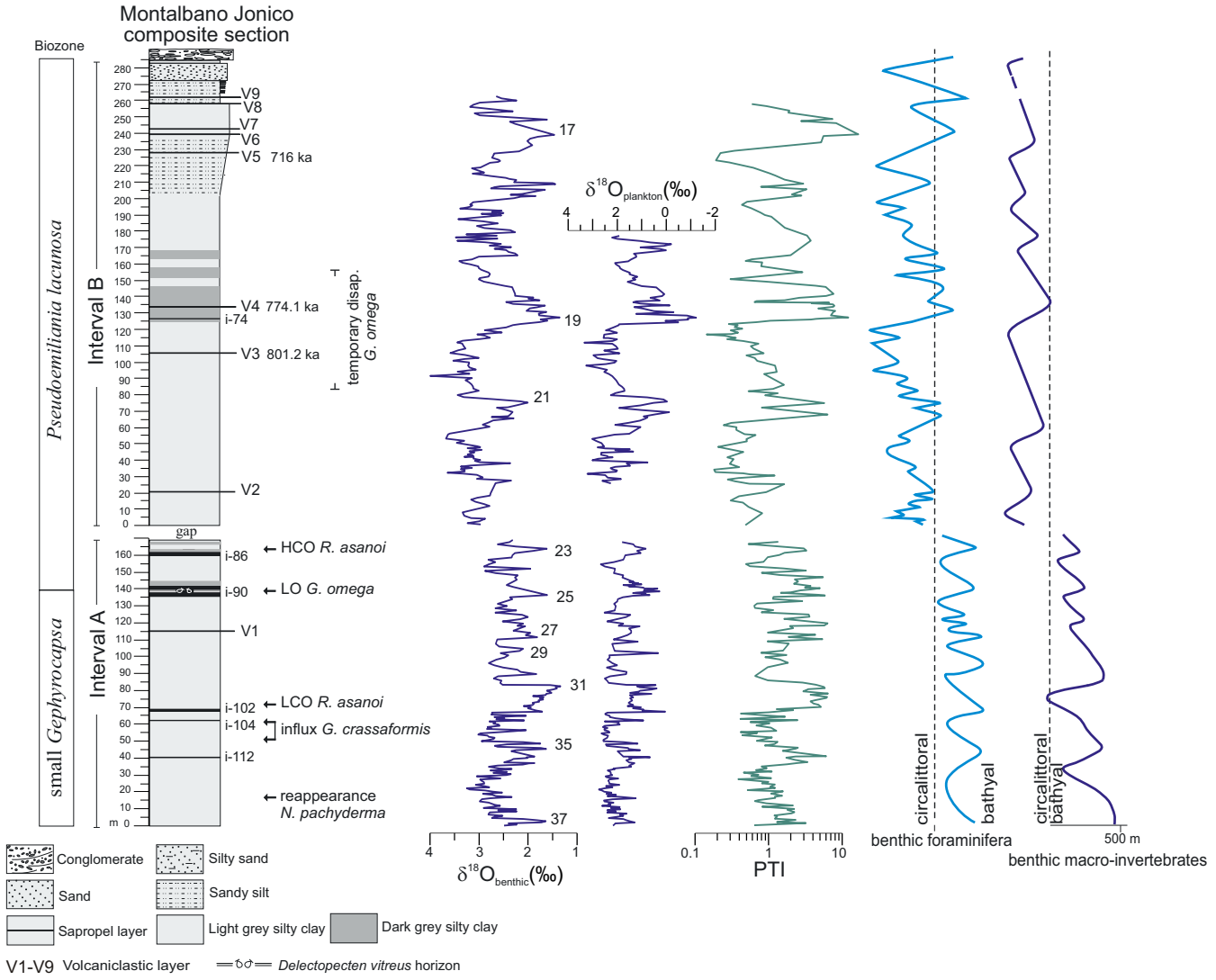

Figure 2. Lithological and stratigraphical features of the composite Montalbano Jonico section (Intervals A and B). Biostratigraphical and paleonvironmental details are traced according to Ciaranfi et al. (2001, 2010), Stefanelli (2003, 2004), D'Alessandro et al. (2003), Maiorano et al. (2004, 2010) and Girone et al. (2013). $\delta^{18}O_{planktonic}$ and $\delta^{18}O_{benthic}$ are from Brilli (1998), Brilli et al. (2000) and Ciaranfi et al. (2010). Pollen Temperature Index (PTI) record (in logarithmic scale) derives from Mesothermic/Steppic taxa ratio and is from Joannin et al. (2008) for Interval A, Vannacci (2016) for MIS 22, Bertini et al. (2015) and Toti (2015) for the MIS 21–17 interval. LO: Lowest Occurrence; HO: Highest Occurrence; LCO: Lowest Common Occurrence; HCO: Highest Common Occurrence. $^{40}Ar/^{39}Ar$ ages of V3–V5 from Ciaranfi et al. (2010), Maiorano et al. (2010), Petrosino et al. (2015), Nomade et al. (2019), and this study.

The MJS, in its lower part (Interval A), includes five sapropel layers (Fig. 2) (D'Alessandro et al., 2003; Stefanelli, 2004; Stefanelli et al., 2005; Maiorano et al., 2008) that are correlated, from the oldest to the youngest, to insolation cycles i-112, i-104, i-102, i-90, and i-86, based on the Mediterranean sapropel stratigraphy of Lourens (2004) and Lourens et al. (2004). In addition, an analogue of the "red interval" ("ghost sapropel", Emeis et al., 2000) correlated to i-74, has been recorded in Interval B of the MJS, based on micropaleontological indications (Maiorano et al., 2016; Marino et al., 2020) and the pattern of the benthic $\delta^{13}C$ record (Nomade et al., 2019). The calcareous nannofossil biostratigraphy indicated that the succession belongs to the small *Gephyrocapsa* and *Pseudoemiliania lacunosa* zones, based on the biostratigraphic scheme of Rio et al. (1990) (Fig. 3). This is equivalent to the CNPL9 and CNPL10 biozones of Backmann et al. (2012) and Raffi et al. (2016), that rely on worldwide biohorizons (Fig. 3). High-resolution quantitative analyses of calcareous plankton assemblages reveal numerous additional bioevents throughout the section (Fig. 3) (Marino, 1996; Marino et al., 2020; Ciaranfi et al., 1997, 2010; Maiorano et al., 2004, 2010, 2016, 2021; Girone et al., 2013). The calcareous plankton bioevents have high correlation potential, being recognized at global scale (Maiorano and Marino, 2004; Maiorano et al., 2010; Backman et al., 2012; Raffi et al., 2006, 2016) (Fig. 3). A detailed biochronology is provided in Table I.

Several deepening-shallowing cycles, from bathyal to circalittoral environments, have been recognized based on micro- and macroinvertebrate benthic assemblages (Fig. 2) (D'Alessandro et al., 2003; Stefanelli, 2003; Ciaranfi and D'Alessandro, 2005; Girone, 2005). Specifically, benthic paleocommunities from the lower part of the succession

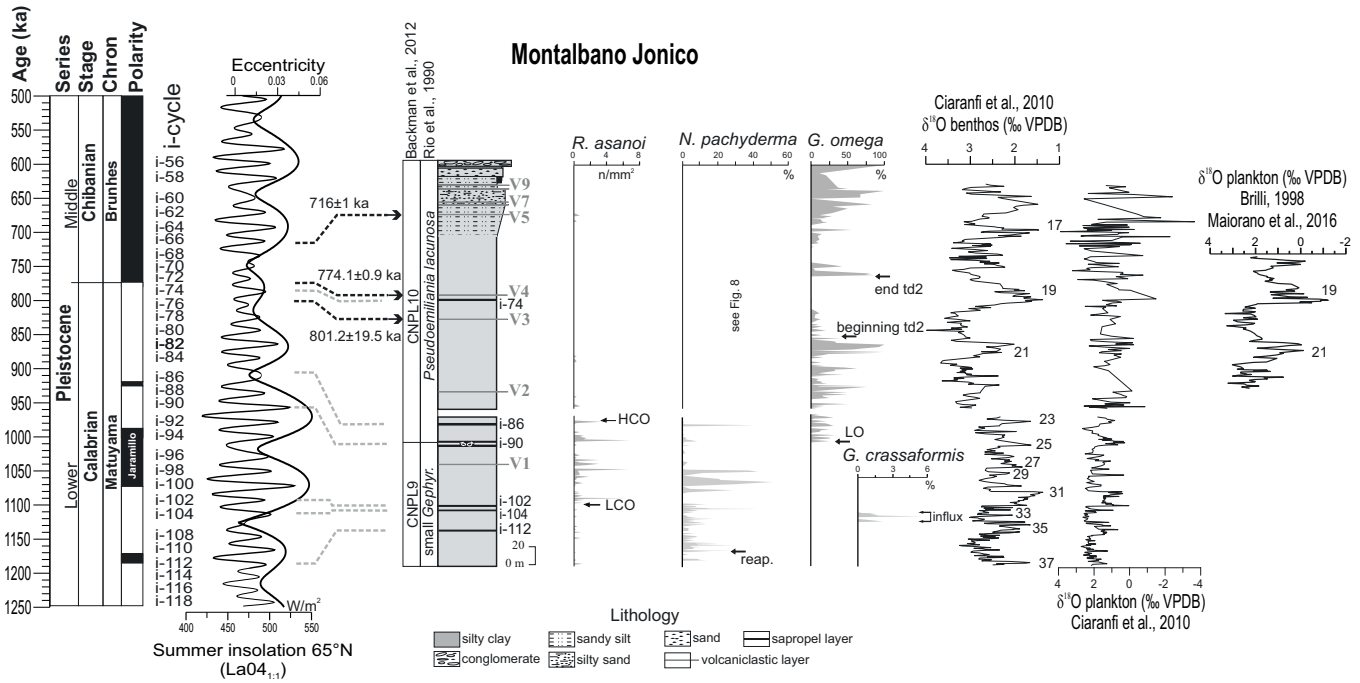

Figure 3. Abundance patterns and bioevents of calcareous plankton index species, oxygen isotope stratigraphy and correlation of sapropel layers of the Montalbano Jonico composite section to summer insolation at 65°N and eccentricity from Laskar et al. (2004) and sapropel stratigraphy from Lourens (2004) and Lourens et al. (2004). LO: Lowest Occurrence; HO: Highest Occurrence; LCO: Lowest Common Occurrence; HCO: Highest Common Occurrence; reap: reappearance. Ar/Ar ages of tephra layers are from Ciaranfi et al. (2010); Maiorano et al. (2010), Petrosino et al. (2015), Nomade et al. (2019), and this study. Chronostratigraphy from Cohen et al. (2013 updated). Modified from Maiorano et al. (2010).

(Interval A) are indicative of a bathyal environment, with a maximum depth of ca. 500 m, while paleocommunities from the upper portion (Interval B) indicate circalittoral settings with short-term deepening towards bathyal (Fig. 2). The whole section represents the regressive part of a third-order cycle, with several fourth- and fifth-order cycles mainly driven by climate changes (Ciaranfi et al., 1994, 1997, 2001, 2010). The onland climate imprint at the glacial–interglacial timescale is wonderfully reflected by the pollen PTI curve (Pollen Temperature Index, sensu Joannin et al., 2008 and Suc et al., 2010) (Joannin et al., 2008; Bertini et al., 2015; Toti, 2015; Vannacci, 2016), which co-varies with $\delta^{18}O$ oscillations and paleodepth variations (Fig. 2).

Stable oxygen isotope analyses performed throughout the entire succession on planktonic (*Globigerina bulloides*) and benthic (*Cassidulina carinata*) foraminifer tests (Figs. 2–3), combined with calcareous plankton biostratigraphy, show that the section encompasses MIS 37 to early MIS 16 (Brilli, 1998; Brilli et al., 2000; Maiorano et al., 2004, 2010; Ciaranfi et al., 2010). Clumped-isotope temperature and $\delta^{18}O_{SW}$ records across several glacial and interglacial cycles from MIS 36 to MIS 19 have been reconstructed (Peral et al., 2020). Average sub-surface temperatures from benthic foraminifer analyses of 13.8 ± 1.5 ℃ and 14.8 ± 1.3 ℃ have been recorded during the climate optima of MIS 31 and MIS 19, respectively. The isotopic composition of seawater in the same intervals has shown values between 1.6 ± 0.4‰ and 2.0 ± 0.3‰, respectively, similar to those measured today below the thermocline in the Gulf of Taranto. The bottom water temperatures in all the glacial periods (MIS 20, 22, 30, 34, 36) were ~ 8 ℃ on average, suggesting that oceanographic conditions in the central Mediterranean Sea were relatively stable before and after the mid-Pleistocene transition at the MJS (Peral et al., 2020).

The benthic and planktonic $\delta^{18}O$ records, combined with biostratigraphy, radiometric data and sapropel stratigraphy, allow the astronomical calibration of the MJS (Ciaranfi et al., 2010; Maiorano et al., 2010, 2016; Marino et al., 2015, Fig. 4). The MJS together with the Vrica-Crotone section (both astronomically-tuned, Lourens et al., 2004, and reference therein; Ciaranfi et al., 2010) cover the whole of Calabrian time, thus representing a potential unit-stratotype for the Calabrian Stage (Maiorano et al., 2010) (Fig. 4). The two onland marine records, when compared with Mediterranean and extra-Mediterranean deep-sea records, support the consistency and reliability of the cyclostratigraphic and biostratigraphic constraints (Maiorano et al., 2010). Both the sections are located in South Italy, a reference region for Quaternary chronostratigraphy, within the Mediterranean area, which is the cradle of most Neogene and Quaternary GSSPs.

The Ideale section as a Standard Auxiliary Boundary Stratotype of Middle Pleistocene

The IS has a thickness of 74.19 m and covers the late MIS 20 to early MIS 18 interval (Fig. 5). The $^{40}Ar/^{39}Ar$-dated V3 and V4 tephra layers, widely visible in the badlands of the Montalbano area, are well exposed in the IS, cropping out at 8.2 m and 36.6 m respectively. The stratigraphical relevance of the IS through the Lower–Middle Pleistocene transition has been extensively outlined in several papers (e.g., Ciaranfi et al., 1994, 2010; Bertini et al., 2015; Marino et al., 2015, 2020; Maiorano et al., 2016, 2021; Simon et al., 2017; Nomade et al., 2019).

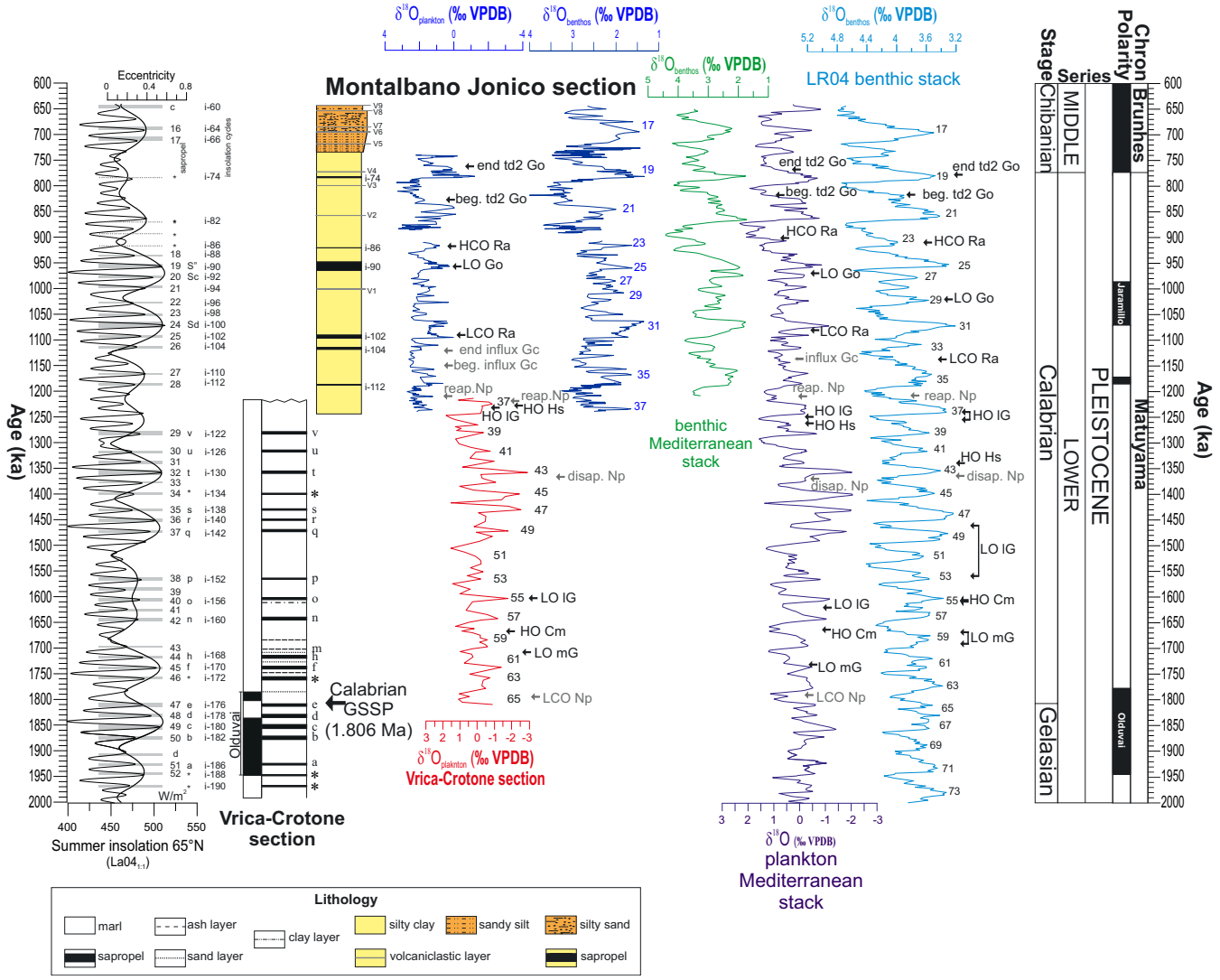

Figure 4. Oxygen isotope chronologies of the astronomically tuned Vrica-Crotone and Montalbano Jonico sections encompassing the entire Calabrian Stage. Position of biohorizons are also traced for comparison on the oxygen isotope Mediterranean stacked record (green line) of Lourens (2004) and on Pacific (Mix et al., 1995a, b; Shackleton et al., 1995) and Atlantic (Bickert et al., 1997) $\delta^{18}O$ benthic records from the biochronology of Lourens et al. (1996, 1998, 2004), Raffi (2002), Maiorano and Marino (2004), Raffi et al. (2006), Ciaranfi et al. (2010). Summer insolation 65°N ($La04_{1,1}$) and eccentricity from Laskar et al. (2004). Np: N. pachyderma; mG: medium Gephyrocapsa; Cm: C. macintyrei; lG: large Gephyrocapsa; Hs: H. sellii; Gc: G. crassaformis; Ra: R. asanoi; Go: G. omega. LO: Lowest Occurrence; HO: Highest Occurrence; LCO: Lowest Common Occurrence; HCO: Highest Common Occurrence; reap.: reappearance; disap.: disappearance; td: temporary disappearance. Chronostratigraphy from Cohen et al. (2013 updated). Modified from Maiorano et al. (2010).

Although lacking a reliable paleomagnetic signal (Sagnotti et al., 2010), the Matuyama–Brunhes transition is recorded at the IS by a ^{10}Be-overproduction interval associated with collapse of the Earth's magnetic field intensity during the MBB, at the MIS 19c/19b transition (Simon et al., 2017; Nomade et al., 2019). A more comprehensive description of the IS is provided below.

Lithostratigraphy

Grain size and mineral content

The Ideale section consists of dark to light grey silty clays (Fig. 5). The main grain size mode (Maiorano et al., 2016, for details) varies from 5.6 to 22 μm, indicating a detrital fraction varying from fine to coarse silt. The clay fraction is generally less abundant in MIS 20 (15–24%, average 19%), whereas it increases significantly (20–31%, average 24%) from the onset of MIS 19 onwards, although several fluctuations have been observed through this interval. Mineralogically, the deposits mainly consist of phyllosilicate minerals, carbonates (calcite and dolomite), quartz and feldspars (see Maiorano et al., 2016 for details). The mineralogical composition and changes, and the grain size variation through the section, are clearly related to the lithological units of the source area and to climate changes. The main increases in quartz and dolomite combined with enhanced supplies of coarser grains, reflect an increase in the coarser detrital mineral components entering the basin during cold phases. During warm phases,

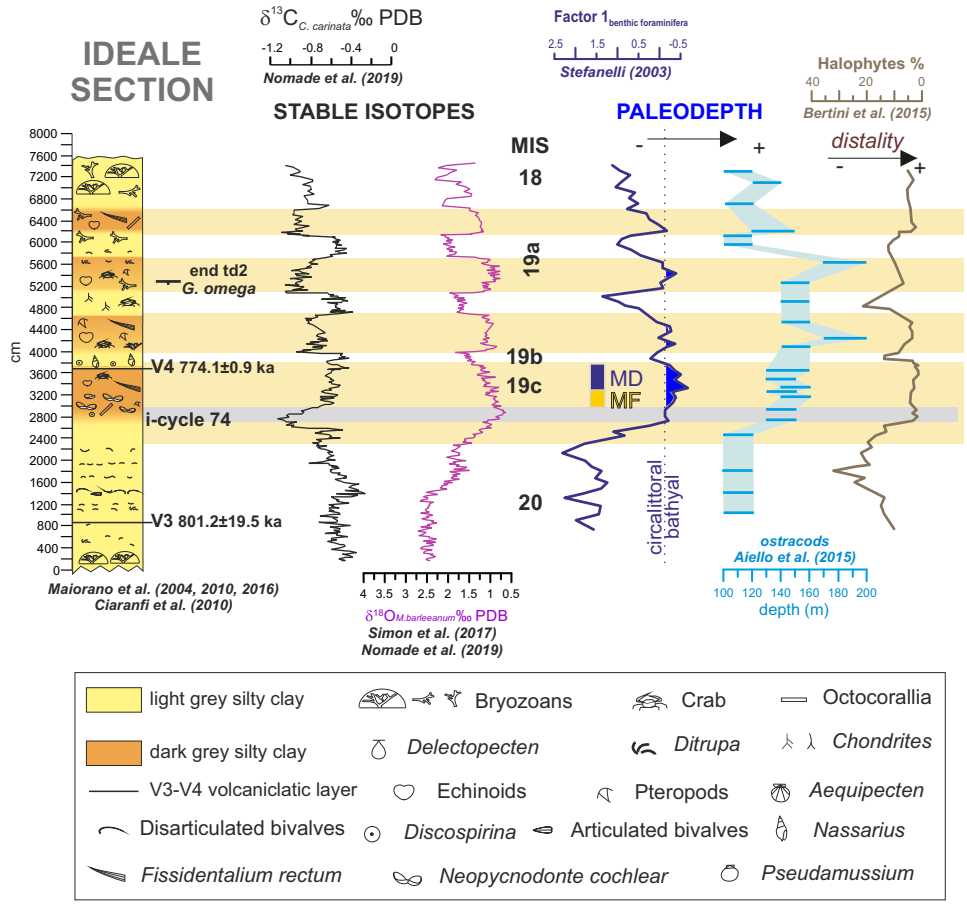

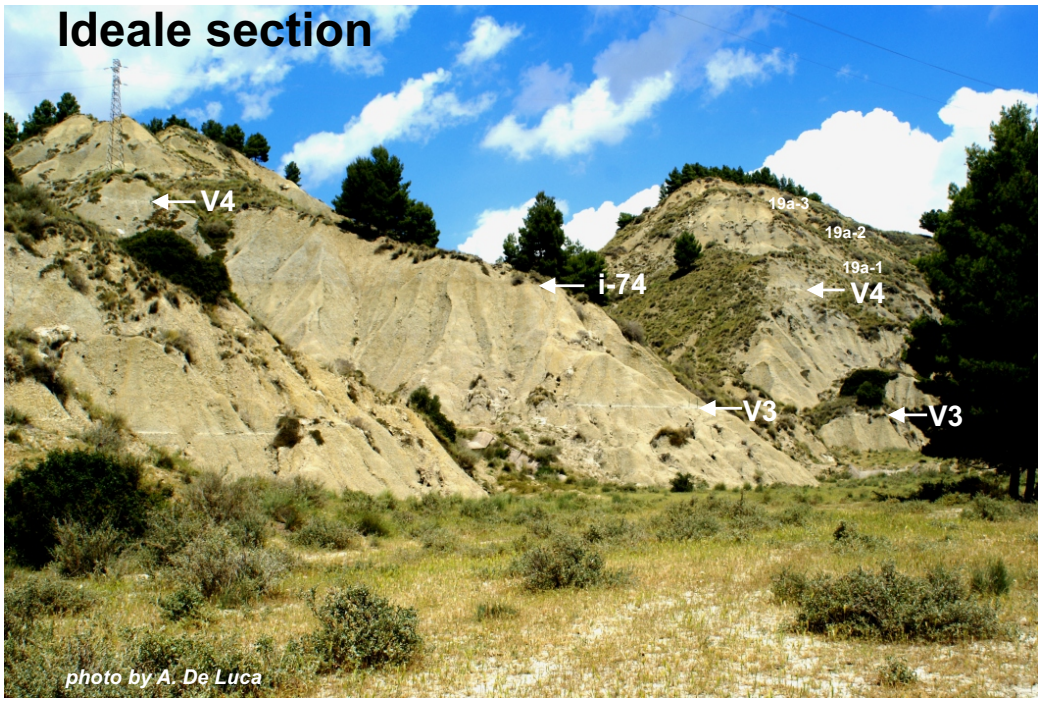

Figure 5. Stratigraphic log of the Ideale section showing the high-resolution stable oxygen and carbon isotopes correlated with the main paleodepth proxies from published data. I-cycle 74 corresponds to the sapropel layer in early MIS 19c. Marine isotope stages and substages and interstadials in MIS 19a are based on Nomade et al. (2019). The "end td2" is end of temporary disappearance of G. omega (Maiorano et al., 2004). MD (maximum depth) and MF (maximum flooding) according to D'Alessandro et al. (2003). Simplified from Marino et al. (2015) and Nomade et al. (2019). A panoramic view of the Ideale section outcrop is shown on the bottom of figure.

higher kaolinite and smectite contents formed, as chemical weathering increased, in good agreement with pollen-derived climate data and the oxygen isotope record (Bertini et al., 2015; Maiorano et al., 2016; Nomade et al., 2019). Such variations correspond to the light and dark grey bands, visible in the Ideale section (Fig. 5), starting from the onset of MIS 19 up to the MIS 18 inception, with darker grey deposits corresponding to wetter and warmer periods.

Tephra layers and $^{40}Ar/^{39}Ar$ age

The V3 tephra layer falls within the MIS 20 interval (at 820 cm) and V4 at the transition from MIS 19c to MIS 19b (at 3,660 cm). V3 is less than 5 cm thick and is a silty sand-sized grey layer with a clayey matrix. The V4 layer is ~10 cm thick and is a silt-sized yellowish grey layer with a clayey matrix. For the $^{40}Ar/^{39}Ar$ age assignment, well preserved sanidine grains from the V3 tephra were selected and analyzed at the Department of Geology and Geophysics (University of Wisconsin in Madison) using a Mass Analyzer Products 215–50 mass spectrometer, following the methods of Meyers et al. (2012). Irradiation, analysis and general interpretive principles are described in detail in Smith et al. (2008). The age uncertainties reported in Petrosino et al. (2015) reflect internal/analytical contributions only at the 2σ level. Sanidine grains from the V4 layer were analyzed at the University of Wisconsin-Madison (USA) using a 60 WCO2 laser and a Nu instruments Noblesse multi-collector mass spectrometer equipped with a Faraday detector and four ETP ion-counting electron multipliers: two at high mass (IC0 and IC1) and two at low mass (IC2 and IC3) positions (Petrosino et al., 2015). Sanidine grains from four kg of the V4 tephra layer were subsequently selected and analyzed (Nomade et al., 2019) at CEA Saclay (France) with a mass spectrometer using a VG5400 equipped with an electron multiplier Balzers 217 SEV SEN coupled to an ion counter. Nomade et al. (2019) used the same crystal age standardization employed in Petrosino et al. (2015), i.e. "astronomical calibration" with the ACs-2 flux standard age at 1.1864 Ma (Jicha et al., 2016) with the total decay constant of Min et al. (2000). All crystals analyzed from both studies were considered as a single dataset, being collected from the same level and exposure, and the weighted mean age of all crystals extracted from V4 (excluding xenocrystic contamination) furnished an age of 774.1 ± 0.9 ka (2σ analytical uncertainty, Nomade et al., 2019 for details).

In tephra V3 and V4, the crystal lithological component, consisting of feldspar, clinopyroxene, brown mica and minor hauyne and garnet, together with non-volcanic gypsum crystals, dominates over the very sparse juvenile fraction. V3 contains poorly preserved vesicular pumice fragments finer than 250 μm, phonolitic in composition. The rare glass particles from the V4 tephra that survived pretreatment are highly altered pumice fragments finer than 250 μm, with elongated vesicles, phonolitic in composition (Petrosino et al., 2015). The Vulture stratovolcano (Fig. 1A) is likely the source of the V3 and V4 tephra, which would represent its oldest dated products (Petrosino et al., 2015, for details).

Biostratigraphy

The calcareous plankton biostratigraphic features of the IS agree with the regional and global pattern occurring across the MIS 20–MIS 18 interval (e.g., Rio et al., 1990; Backman et al., 2012). Furthermore, the temporary disappearance of the calcareous nannofossil *Gephyrocapsa omega* (td2 in Maiorano and Marino, 2004) is extensively documented as an additional biohorizon in the Mediterranean area and the North Atlantic Ocean (Figs. 3–4). In detail, the beginning and the end of td2 are always recorded in MIS 20/21 and MIS 18/19, respectively (Maiorano et al., 2010); the slightly diachronous character of these bioevents may be related to environmental features, although the possibility that this apparent diachroneity could be associated with inconsistencies in age-models cannot be excluded. At the MJS section the age-assignments of the beginning and end of td2 are 0.83 Ma and 0.766 Ma, respectively, based on the age model of Nomade et al. (2019) (Table 1). The end of td2 occurs in the IS at 53.5 m within interstadial MIS 19a-2 (Fig. 5).

Oxygen and Carbon Isotope Records

Low-resolution *C. carinata* and *G. bulloides* $\delta^{18}O$ records spanning the entire MJS have been published by Brilli et al. (2000), Ciaranfi et al. (2010), and Maiorano et al. (2016; with references therein) (Fig. 2). The IS has been subsequently re-sampled at very high resolution (1 sample every 20 cm, ~90–200 years) thus providing excellent $\delta^{18}O_{M.\ barleeanum}$ and $\delta^{18}O_{C.carinata}$ and $\delta^{13}C_{C.carinata}$ records covering MIS 20 to MIS 18 (Simon et al., 2017; Nomade et al., 2019), based on 353 samples (Fig. 5). The analyses were performed on a GV-Isoprime dual-inlet gas mass spectrometer at the LSCE laboratory. All results are expressed as $\delta^{18}O$ and $\delta^{13}C$ vs VPDB (in ‰) with respect to NBS 19 standard. The internal analytical reproducibility determined from replicate measurements of a carbonate standard is ±0.05% (1σ). Here the $\delta^{18}O_{M.\ barleeanum}$ and $\delta^{13}C_{C.carinata}$ records are reported (Fig. 5).

Values of $\delta^{18}O_{M.\ barleeanum}$ vary between ~0.6 and 2.6‰. This record shows that the IS provides a very detailed marine isotopic record of Termination IX (TIX) and extends upwards into MIS 18. The deglaciation interval is 16 m thick, recorded between 1,240 and 2,860 cm. It corresponds to a decrease of nearly 2‰ in the $\delta^{18}O$ values, which range from ~2.6‰, at the glacial maximum, to ~0.6‰ at the peak of MIS 19c (Fig. 5). From the peak value of MIS 19c, at ~2,860 cm, the benthic $\delta^{18}O$ record shows a generally progressive increase upwards with minor oscillations until about 3640 cm, followed by a rapid increase and climate degradation starting at 3,715 cm up to the value of 1.83‰ at 3,975 cm (MIS 19b) (Fig. 5). Then, the $\delta^{18}O$ record shows an extremely abrupt decrease, with values dropping by more than 0.7 ‰ (from 1.83 to 1.10‰) in only 40 cm, and by ~1‰ in one meter (Fig. 5). This abrupt shift marks the upper portion of the study record, which is characterized by relatively stable intervals with low $\delta^{18}O$ values (suggesting a return to warm/wet conditions), limited by extremely abrupt $\delta^{18}O$ changes towards more positive values (cooler and/or drier conditions) (Fig. 5). Three warmer/wetter episodes (interstadials 19a-1, 19a-2, 19a-3) are clearly visible in the $\delta^{18}O$ record (at 3,975–4,656 cm, 5,049–5,718 cm, and 6,119–6,639 cm, respectively) (Fig. 5). A shorter warm episode is recorded higher, between 6,812 and 7,072 cm and it may correspond to the fourth interstadial in MIS 19a according to Haneda et al. (2020a) and Head et al. (2021). Upwards, the isotopic record reveals heavier $\delta^{18}O$ values with the maximum (2.3‰) at 7115 cm, interpreted as belonging to MIS 18 (Fig. 5) (Nomade et al., 2019).

The very high-resolution $\delta^{18}O$ curve at the IS has provided one of the most detailed records of the MIS 20–MIS 18 interval and of Ter-

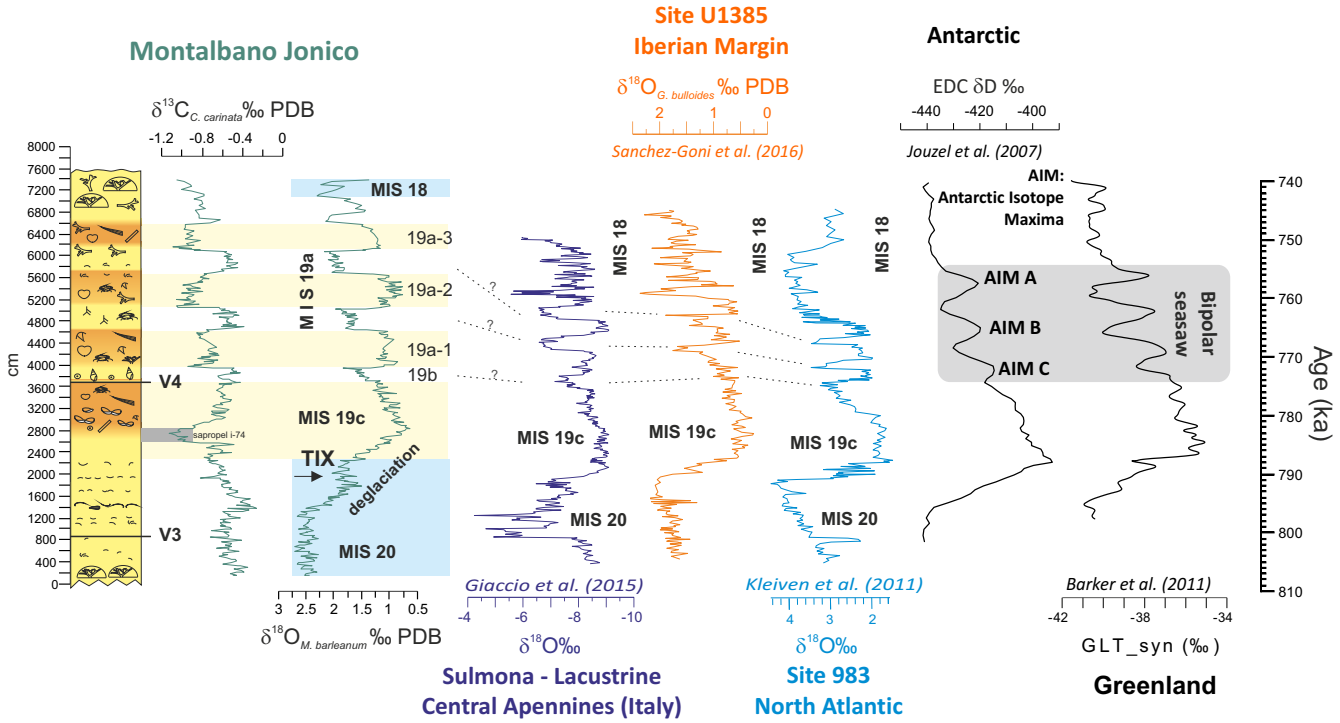

Figure 6. $\delta^{18}O_{M.barleeanum}$ and $\delta^{13}C_{C.carinata}$ records (vs depth) from the Ideale section and compared with other high-resolution worldwide climate records (vs time). Glacials MIS 20 and 18, and interglacial substage MIS 19 in the IS are based on Nomade et al. (2019). GL_T-syn: synthetic climatic record from Greenland. For lithological/paleontological features of the Ideale section see legend in Fig. 5.

mination IX worldwide (Fig. 6). The rapid oscillations observed above MIS 19c resemble those recorded in the isotopic record of Sulmona paleolake (central Italy, Giaccio et al., 2015; Regattieri et al., 2019), and in the $\delta^{18}O$ records from the North Atlantic (Channell et al., 2010; Ferretti et al., 2015; Sánchez Goñi et al., 2016), in the δD pattern from EPICA Dome C (Pol et al., 2010), and in the synthetic climatic record from Greenland (GL_T-syn), based on the thermal bipolar seesaw model (Barker et al., 2011; Tzedakis et al., 2012) (Fig. 6) discussed in Nomade et al. (2019) and Head (2021). These oscillations crucially are also represented within the Chiba composite section (Suganuma et al., 2021; Head, 2021). Therefore, the $\delta^{18}O_{benthic}$ oscillations of the IS from MIS 19c upwards record a global signal (i.e., global ice volume) despite being from a shallow-water environment (180–200 m depth maximum, Fig. 5, Aiello et al., 2015).

The $\delta^{13}C$ record varies from ~ 0.45‰ to ~ 0.75‰ during the deglaciation, corresponding to a net decrease of 0.3‰, which is equivalent to the global $\delta^{13}C$ effect known for the last deglaciation (TI, Köhler et al., 2005). An abrupt drop in $\delta^{13}C$ (by ~0.4‰ to reach ~ 1.15‰ in less than 40 cm, ~200 years) may be observed in the final part of the deglaciation. The interval at the end of deglaciation (from ~2,540 cm to 2,960 cm) is characterized by low $\delta^{13}C$ values. This low-$\delta^{13}C$ interval has been associated with a sapropel layer, in agreement with micropaleontological evidence (Maiorano et al., 2016; Marino et al., 2020). This sapropel provides a very useful constraint for constructing the age model of the IS based on orbital tuning considerations and radiometric ages of V3 and V4. The rapid oscillations observed in the $\delta^{18}O$ record of MIS 19b-a (Fig. 5) are associated with clear variations in $\delta^{13}C$, which suggest a direct response of productivity, organic matter of terrestrial origin, water column structure and sea bottom ventilation to rapid climatic change during the precession minimum (Nomade et al., 2019; Maiorano et al., 2021).

The Matuyama–Brunhes Boundary and Authigenic $^{10}Be/^{9}Be$ Ratio

Paleomagnetic results are not helpful at MJS due to complete remagnetization resulting from late-diagenetic greigite growth (Sagnotti et al., 2010). Along with paleomagnetic measurements, cosmogenic radionuclide beryllium-10 (^{10}Be) in natural archives can provide complementary information on past variations of the geomagnetic field intensity (e.g.,Valet and Fournier, 2016). The first data on authigenic $^{10}Be/^{9}Be$ ratios were provided by Simon et al. (2017). Additional $^{10}Be/^{9}Be$ ratio results (total 193 levels) through the entire IS up to MIS 18 were shown in Nomade et al. (2019). The authigenic $^{10}Be/^{9}Be$ ratio curve reveals a peculiar pattern through the IS yielding a subdivision into 5 phases (Fig. 7). Within phase 1, with the exception of the V3 level, the $^{10}Be/^{9}Be$ ratio has a mean value of $0.24 \pm 0.05 \times 10^{-8}$ and smoothly decreases to 0.08×10^{-8}. This period is followed by a rather constant increase of the $^{10}Be/^{9}Be$ ratio (phase 2) that stabilized at a plateau at $0.37 \pm 0.02 \times 10^{-8}$ within the 3,255–3,411 cm interval. The highest $^{10}Be/^{9}Be$ ratio, corresponding to maximum values of the IS peak, is of $0.55 \pm 0.06 \times 10^{-8}$ within the 3,541–3,645 cm interval (Fig. 7). This represents a near doubling of the $^{10}Be/^{9}Be$ ratio compared to the preceding interval (0.27×10^{-8} from 0 to 3,411 cm). That sequence is followed by a sharp drop in $^{10}Be/^{9}Be$ ratios ($0.20 \pm 0.16 \times 10^{-8}$) associated with sediments deposited during and immediately after the V4

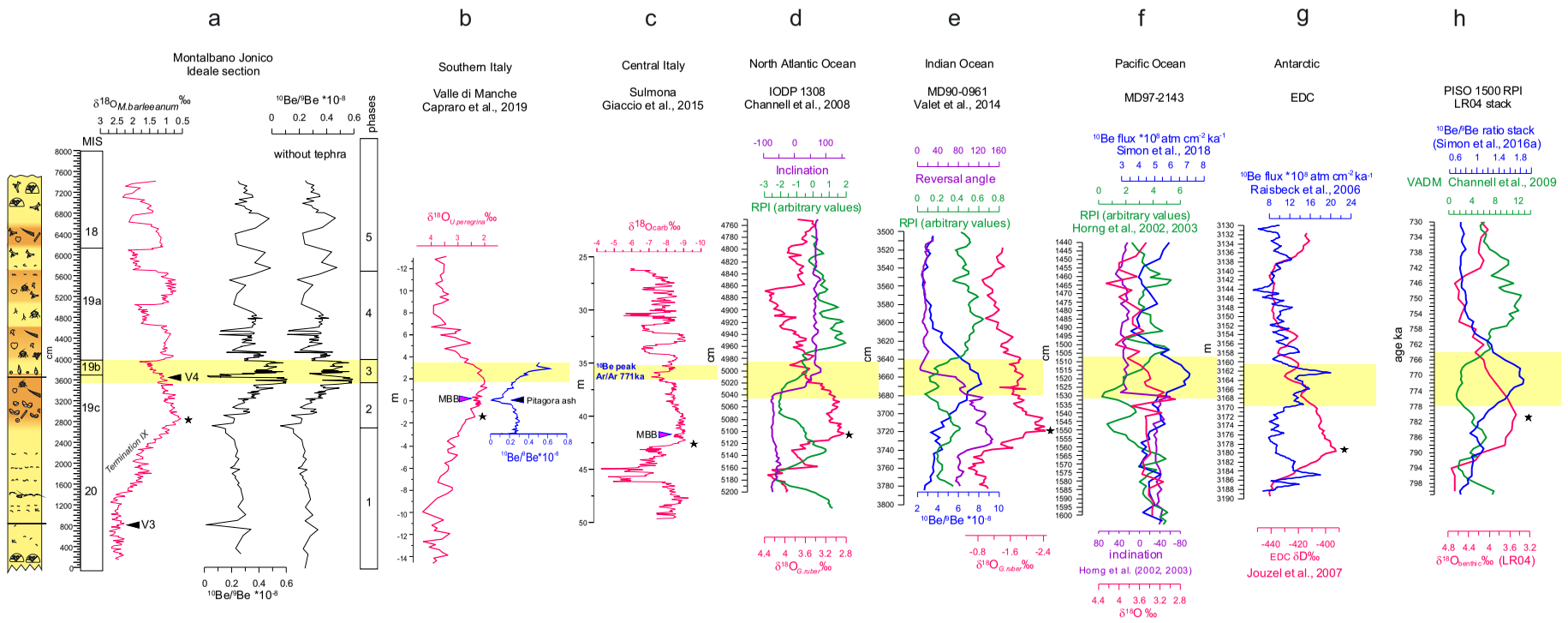

Figure 7. (a) Stratigraphic positioning of the authigenic $^{10}Be/^{9}Be$ ratio (with and without the tephra layers V3 and V4) and benthic $\delta^{18}O$ records from the Ideale section compared to (b) the benthic $\delta^{18}O$ record and the $^{10}Be/^{9}Be$ ratio at Valle di Manche (Capraro et a., 2019), to (c) $\delta^{18}O_{carbonate}$ (Giaccio et al., 2019) and the ^{10}Be peak at Sulmona (Giaccio et al., 2023), and to (d) paleomagnetic results at IODP Site U1308 from the North Atlantic Ocean; (e) authigenic $^{10}Be/^{9}Be$ ratio, planktic $\delta^{18}O$ record and paleomagnetic results at core MD90-0961 from the Indian Ocean; (f) authigenic $^{10}Be/^{9}Be$ ratio, benthic $\delta^{18}O$ record and paleomagnetic results at core MD97-2143 from the Pacific Ocean; (g) δD_{ice} record and ^{10}Be-flux at EPICA Dome C (EDC) from Antarctica; and (h) PISO-1500 RPI stack, LR04 benthic $\delta^{18}O$ stack and equatorial authigenic $^{10}Be/^{9}Be$ ratio stack. The onset of MIS 19c in each series is set using the lightest $\delta^{18}O$ or according to original reference, or lowest δD_{ice} peak. For lithological/paleontological features of the Ideale section see legend in Fig. 5.

event (Fig. 7), such as at the V3 level. The authigenic ^{9}Be inputs associated with tephra layers V3 and V4 are related to direct mantle inputs and/or very dense particulate environments following the fallout of pyroclastic flow, that contributes to drastically modifying the concentrations, scavenging rates and/or mixing of dissolved Be in the water column. Thus, we excluded the tephra layers from the geomagnetic ^{10}Be/^{9}Be ratio interpretation given the peculiar geochemical behavior of dissolved Be isotopes within these specific intervals. A similar observation was made at the Valle di Manche section (Capraro et al., 2019). When removing the layer disturbed by the tephra signal, the highest ^{10}Be/^{9}Be ratio values from the IS, i.e. 0.58 ±0.01 ×10^{-8}, is within the 35.50–39.50 cm interval (phase 3). During phase 4 the authigenic ^{10}Be/^{9}Be ratios return to an average mean of 0.28 ±0.08 ×10^{-8}, consistent with values recorded before the major enhancement of phase 3. Phase 5 is characterized by two ^{10}Be/^{9}Be ratio increases (Fig. 7) associated with period of enhanced erosion of carbonate (dolomitic) and sandstone bedrock units, supply of coarser sediment, and coccolith reworking during cold periods (Maiorano et al., 2016; Fig. 2 in Simon et al., 2017). Except for this specific interval, the absence of correlation with environmental proxies or sea level changes (Fig. 2 and Table S2 in Simon et al., 2017) supports a geomagnetic interpretation of the authigenic ^{10}Be/^{9}Be ratio fluctuations in the IS.

The high ^{10}Be/^{9}Be ratio values (^{10}Be overproduction episode, Simon et al., 2017) from phase 3 result from low geomagnetic dipole moments at the MBB interval. This ^{10}Be overproduction episode begins during late MIS 19c and extends over the MIS 19b period, according to the high-resolution benthic oxygen isotope record at the IS (Fig. 7) (Nomade et al., 2019). As discussed in Simon et al. (2017), when the authigenic ^{10}Be/^{9}Be ratio from the IS is compared to climatostratigraphic and paleomagnetic proxies of global marine and ice-core records, its increase interval is consistent with the RPI drop at the late MIS 19c–early MIS 19b interval (Fig. 7). Such a ^{10}Be/^{9}Be datum is comparable to that recorded in all available ^{10}Be records, including the Sulmona and Valle di Manche records, and within the Chiba composite section in which the MBB is recorded, and Middle Pleistocene GSSP is defined (Suganuma et al., 2021).

The position of the cosmogenic ^{10}Be peak in the lacustrine Sulmona record and marine Valle di Manche section is represented in Figure 7. The abrupt end of the ^{10}Be peak occurs at 771 ka in the Sulmona section (Giaccio et al., 2023) while the MBB is dated at 786.1 ± 1.5 ka (Sagnotti et al., 2014, 2016). The ^{10}Be/^{9}Be ratio at Valle di Manche has its highest values in late MIS 19c, while the paleomagnetic VGP latitudes and magnetic DGRM/DNRM parameter indicate the MBB in the lower MIS 19c at 786.9 ± 5 ka (Capraro et al., 2017, 2019; Macrì et al., 2018). These chronostratigraphic offsets between directional change (often chosen to pinpoint reversals) and dipole moment drop might result from globally asynchronous directional reversal features associated with a non-dipolar transitional field component (Singer et al., 2019), by unreliable records of transitional directions in low sedimentation rate sequences (Valet et al., 2016), and/or by late magnetization or remagnetization issues (e.g. Roberts et al., 2010).

Age Model

An astronomical calibration of the entire Lower–Middle Pleistocene composite section of Montalbano Jonico was given in Ciaranfi et al. (2010) (Figs. 4–5). This first chronology of the MJS rests upon (i) the tuning of 5 sapropels to insolation cycles i-112, i-104, i-102, i-90 and i-86, and (ii) the correlation of the MJS low-resolution planktonic δ^{18}O record with astronomically-tuned ODP Site 975 isotopic stratigraphy (Lourens et al., 2004). In addition, a ^{40}Ar/^{39}Ar age of 719.5 ± 12.6 ka was obtained for tephra V5 (Ciaranfi et al., 2010).

Later, the chronological framework of the IS alone was revised by using ^{40}Ar/^{39}Ar ages for the V3 and V4 tephras (Maiorano et al., 2010; Petrosino et al., 2015) and by tuning the benthic δ^{18}O record to the LR04 benthic stack of Lisiecki and Raymo (2005) (Marino et al., 2015). However, recent evidence suggests that tuning benthic δ^{18}O records to a unique global reference curve such as the LR04 stack neglects regional diachroneity (Lisiecki and Stern, 2016). In the Mediterranean basin, those potential diachroneities can result in 2–3 ka offsets between the age assignment of major isotopic features at glacial terminations (max. bias ~9 ka for termination TVII, Konijnendijk et al., 2015), and their counterparts in the LR04 stratigraphy.

To bypass that issue, Simon et al. (2017), based on resampling of the IS at centennial-scale resolution, set up a regional strategy for developing an accurate astronomically-derived age model for MIS 20–MIS 19. Simon et al. (2017) assumed that climate changes across TIX may have been similar (major features, phase) to those recorded across TI (Tzedakis et al., 2012; Giaccio et al., 2015; Yin and Berger, 2015). They used well-dated (AMS ^{14}C) δ^{18}O isotopic records covering the last deglaciation in the vicinity of the Ionian Sea (cores MD90-917, MD90-918, Siani et al., 2004; Caron et al., 2012), in order to decipher precisely the phase relationship between climatic changes and insolation and they applied it to phase-lock TIX relative to insolation. The age-model was settled by linear interpolation adding the age of V4 at 773.9 ka (Petrosino et al., 2015) as an additional tie-point.

Following the age model proposed by Simon et al. (2017), further improvement was provided by Nomade et al. (2019) based on the high-resolution sampling of a longer sedimentary record extending up to MIS 18 and applying a minor correction to the thickness of the IS above V4. This has been possible owing to the study of the contemporaneous and continuous CM section outcropping in the Montalbano Jonico badlands (Fig. 3 in Nomade et al., 2019). The new age model of Nomade and co-authors is a hybrid chronology, which includes both astronomical tie-points (the onset of deglaciation dated at 794 ka, the onset of sapropel i-c 74, dated at 785.4 ka - i.e. a phase lag of 3 ka relative to maximum northern insolation in June; Langereis et al., 1997; Lourens, 2004, the onset of MIS 18 astronomically dated at 757 ka) and the dated tephra layers V3 (801.2 ± 18.5 ka) and V4 (774.1 ± 0.9 ka) (Fig. 6 in Nomade et al., 2019). This hybrid age model, following a Bayesian approach, gives i) a duration of 13.7 kyr for MIS 19c and of 11.5 kyr (95% confidence) for the full interglacial MIS 19c (climate optimum); ii) a duration of ~2.5 kyr (785.0–782.5 ka) for the sapropel-like event in the lower MIS 19c, synchronous with i-cycle 74 (784 ka, Langereis et al., 1997; Lourens, 2004); iii) a duration of ~1.2 kyr for MIS 19b; iv) an average duration of ~5.4 kyr for the sub-orbital MIS 19a interstadials. With the hybrid age model tuning solution, the three rapid oscillations observed during MIS 19a are all contained within a single precessional cycle (Fig. 8). The high resolution of the IS makes it possible to address the duration of such rapid oscillations that are very rapid (i.e., <200 years); the average ~5.4 ka duration of the sub-orbital MIS 19a interstadials is in good accordance with the results

Table 2. Chronological constraints and duration of the main climate phases and events at the Ideale section

Chronological constrains and duration of phases and events at the IS	
	age
V3	$^{40}Ar/^{39}Ar$ 801.2 ± 19.5 ka
sapropel i-74	784 ka
V4	$^{40}Ar/^{39}Ar$ 774.1 ± 0.9 ka
MIS 18 onset	757 ka
	event duration
MIS 19c	13.7 kyr
MIS 19c climate optimum	11.5 kyr
sapropel i-74	~2.5 kyr (785.0–782.5 ka)
Maximum flooding	780–777 ka
Maximum depth	~778–774 ka
MIS 19b	~1.2 kyr (~773.8–772.6 ka)
$^{10}Be/^{9}Be$ ratio	776.35–771.87 ka
MIS 19a interstadials	~5.4 kyr

found by Sánchez-Goñi et al. (2016) from the Iberian Margin, as a quarter precessional signal (Ferretti et al., 2015). In detail, spectral analysis on $d^{18}O$ of IS extracted a prominent millennial cyclicity at 5.4 ka using the Bayesian hybrid age-model, similar to cyclicity from the $\delta^{18}O_{carbonate}$ record of the Sulmona paleolake (5.9 ka, Giaccio et al., 2015) (Fig. 7 in Nomade et al., 2019).

Finally, the ^{10}Be overproduction episode associated with the MBB is dated at 776.35–771.87 ka (Nomade et al., 2019). The timing of the geomagnetic intensity collapse episode is consistent with paleomagnetic measurements from globally distributed marine and lava records, with ^{10}Be-proxies from all existing marine records, as well as with the ^{10}Be-flux peak observed in the EPICA Dome C records (Fig. 7). By using only a few tie-points in the hybrid age model, it is not possible to properly resolve all sedimentation rate changes that may have occurred during MIS 19 at the IS (Fig. 6 in Nomade et al., 2019); the age uncertainties estimated across this time period, varying from 3.4 up to 6.3 ka, are the same occurring in any age model that is constrained by a limited number of tie-points, absolute or not (Nomade et al., 2019). The newly obtained age of V5 (S1–S3) is not considered here for IS chronology despite being extremely precise because it is far too young and does not change the age model around the MBB proposed by Nomade et al. (2019).

In Table 2 the main chronological data at the IS are summarized.

Paleoenvironmental Reconstruction of the Ideale Section

In the IS, multiple paleontological proxies from both marine and terrestrial realms combined with geochemical signals and marine biomarkers provide a clear framework of paleoenvironmental evolution and a series of changes related to regional and global climate variations (Figs. 5–8).

Paleodepth Reconstruction

The relative paleodepth throughout the IS varies from about 100 m to 180–200 m based on ostracod assemblages (Aiello et al., 2015); although at low sampling resolution, an upper Lower Circalittoral Subzone (LCS, sensu Sgarrella and Moncharmont-Zei, 1993) ostracod association is recorded in the upper MIS 20 (Fig. 5). The paleodepth increase begins from 2700 cm (ostracofauna), nearly concurrent with an increase in distality (decrease of halophyte plants – e.g. Amaranthaceae, Caryophyllaceae, *Ephedra* – used in this context as an indirect proxy of sea-level fluctuations and distality changes) (Fig. 5). Such a pattern is concordant with a trend of deepening corresponding to deglaciation recorded by decrease in $\delta^{18}O$ that can be partly attributed to the waning of continental ice caps (Fig. 5). Benthic foraminifera indicate two sea-level minima at 1,370 cm and 2,150 cm, and a prominent deepening trend towards 2,700 cm, matching the $\delta^{18}O$ pattern (Fig. 5). At about 3,000 cm, deepening evidence is also provided by the occurrence of *Funiculina quadrangularis* (D'Alessandro, unpublished; Marino et al., 2015, see references therein). Maximum flooding (MF) was documented by D'Alessandro et al. (2003) between about 3,070 cm and 3,370 cm (Fig. 5) based on the occurrence of scattered clusters of the deep-water oyster *Neopycnodonte cochlear*, a species that thrives during low sedimentation rates and in low turbidity conditions on the sea bottom (Massari et al., 2002; Ceregato et al., 2007; Wisshak et al., 2009) related to rapid sea level rise after deglaciation. The onset of MIS 19c is recorded by the replacing of the upper LCS assemblages with a lower LCS ostracofauna (Fig. 5). The maximum depth interval (MD, from 3,370 cm to 3,770 cm), is characterized by dispersed macrobenthic content and the occurrence of bathyal taxa among foraminifera and ostracods, and, even as rare specimens, in the mollusc assemblage (D'Alessandro et al., 2003). The maximum depth estimated for the IS agrees with the global sea level timing of Elderfield et al. (2012) at around 774 ka (Nomade et al., 2019) (Fig. 8). Benthic foraminifera and halophyte patterns from 3850 cm to 3980 cm indicate decreased paleodepth that is coeval with heavier $\delta^{18}O$ values in MIS 19b. Similarly, the shallowing and deepening phases recorded upwards in pollen, benthic foraminifera and ostracod assemblages are in phase with the $\delta^{18}O$ pattern, attesting to a coherent signal of climate and sea level fluctuations towards the MIS 18 onset (Fig. 5).

Climatostratigraphy

The signature of orbital to millennial climate variability is clearly imprinted in the IS as recorded by multiproxy investigations (Bertini et al., 2015; Marino et al., 2015, 2016; Maiorano et al., 2016, 2021; Nomade et al., 2019; Marino et al., 2020) and most visibly expressed on the exposure by the dark grey and light grey bands, which correspond to the warm-wet and cold-dry climate phases, respectively (Figs. 5–6, 8).

A terminal stadial-like event (Med-H_{TIX}) occurred in late MIS 20 between 794 and 788.5 ka as a result of combined atmospheric dynamics and oceanic/hydrological processes. It is characterized by i) an alkenone-SST 4–5 ℃ cooler than in the older interval, ii) higher abundances of arctic-subarctic *Coccolithus pelagicus* ssp. *pelagicus* and *Neogloboquadrina pachyderma*, iii) a large expansion of open landscapes including prevalent (cold) dry steppe on land (Bertini et al., 2015), and iv) a lightening of 1‰ in the $\delta^{18}O_{M.\ barleeanum}$ reflecting the influx of lighter fresh water into the Ionian Sea (meltwaters coming from mountain glaciers of the Alpine and Apennines chains or from

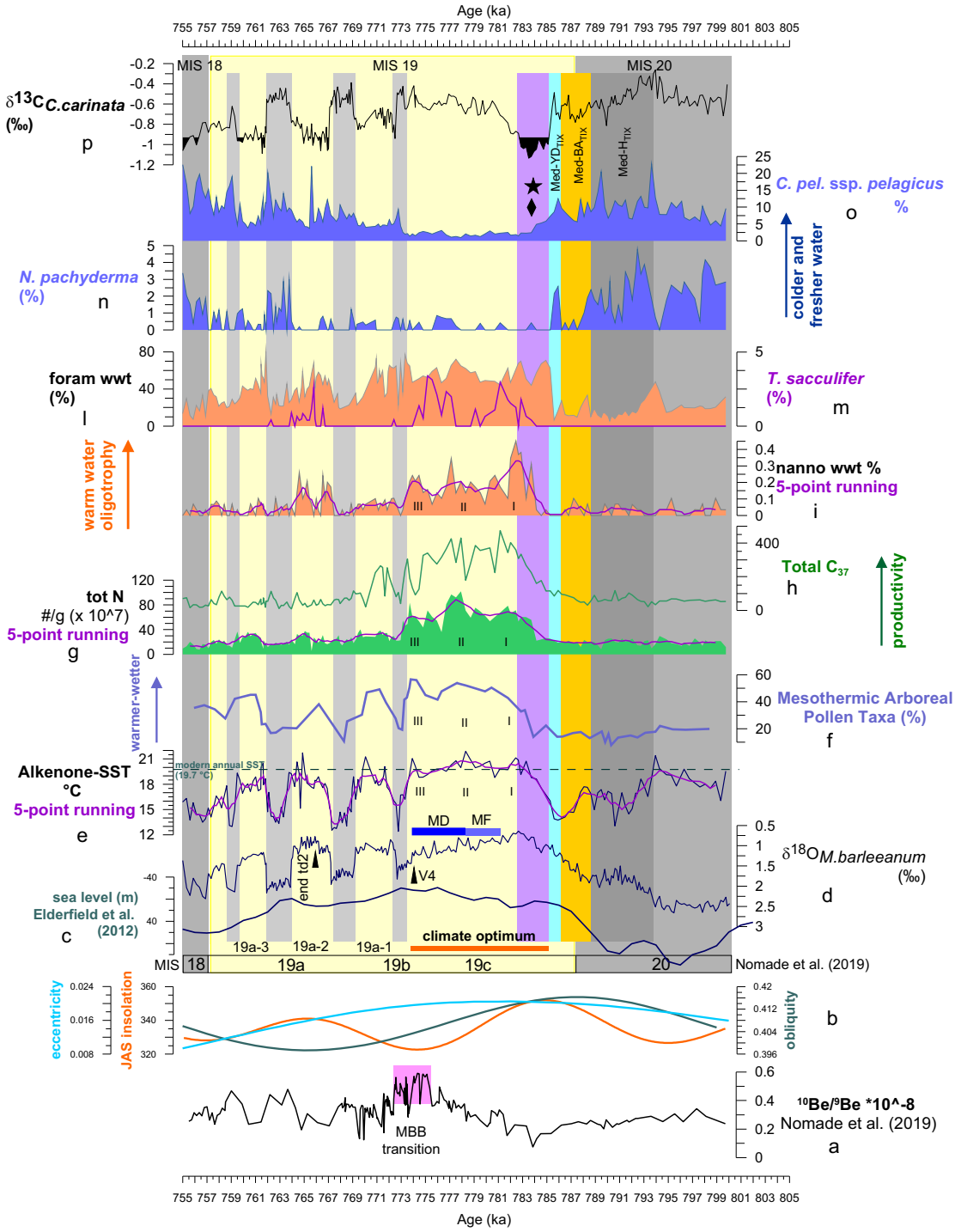

Figure 8. Climatostratigraphic signals at the Ideale section. Quantitative abundance patterns of selected calcareous plankton taxa (i-o) expressed as percentage, alkenone-SST (e), benthic oxygen (d) and carbon isotope (p) records, and Mesothermic Arboreal Pollen Taxa (f). Modern annual SST (19.6 °C) is shown on the alkenone-SST record of Pujol and Vergnaud-Grazzini (1995). Foram wwt (l) and Nanno wwt (i) curves are planktonic foraminifera and calcareous nannofossil warm water taxa, respectively. Tot N (number of coccoliths/g of sediment, #/g), is the total abundance of coccoliths (g). Total alkenones (h) are expressed as ng/g. Mean summer insolation (65° N), obliquity and eccentricity (b) are from Laskar et al. (2004). Sea level curve (c) is from Elderfield et al. (2012). MIS 19a1–19a3 are interstadials during 19a based on Nomade et al. (2019). Stage boundaries and climate optimum are marked according to Nomade et al. (2019). Glacial MIS 20 and MIS 18 intervals are shown by grey bands. Light yellow color marks interglacial and interstadial phases. Light gray bands on proxy records are stadial phases; dark gray, dark yellow, blue bands represent Med-H_{TIX}, Med-BA_{TIX}, Med-YD_{TIX}, respectively. Lilac band is the sapropel i-cycle 74 based on Maiorano et al. (2016) and Nomade et al. (2019). Diamond symbol in sapropel layer is the higher infauna/epifauna ratio in the benthic foraminifera assemblage (Stefanelli, 2003), and the star symbol is the abundance peak of dinocyst P. zoharyi (Bertini et al., 2015; Maiorano et al., 2016). I, II and III on curves e–g and i are the main warmer phases in MIS 19c. $^{10}Be/^{9}Be$ ratio (a) is also shown. Modified from Nomade et al. (2019), Marino et al. (2020) and Maiorano et al. (2021).

North Atlantic via the Gibraltar Strait) (Fig. 8). The Med-H_{TIX} at the IS is not a local episode (Maiorano et al., 2016; Marino et al., 2020). It correlates with a peak of $C_{37:4}$ (low salinity and cold waters) at the Western Mediterranean Site 975 (Quivelli et al., 2021) and at the Iberian Margin IODP Site U1385 (Rodrigues et al., 2017) and has a close temporal relationship with the deposition of ice-rafted debris (IRD) in the northern Atlantic. There, the low $\delta^{13}C_{benthos}$ values at sites 980 (Wright and Flower, 2002) and 983 (Kleiven et al., 2011) suggest water column stratification and shutdown of Atlantic Meridional Overturning Circulation (AMOC) (Fig. 4 in Marino et al., 2020). The multiple sub-millennial oscillations in climate proxies (alkenone-SST, calcareous plankton key taxa) during the Med-H_{TIX} at the IS have been explained as a response to fluctuating Atlantic-Mediterranean hydrological connection in terms of episodic restoration of Modified Atlantic Water and temporary decreases of Atlantic meltwater influxes (Marino et al., 2020).

During Termination IX, short-term episodes before the onset of full interglacial MIS 19c have been identified and compared with the high-frequency climate instability that occurred during Termination I (Maiorano et al., 2016). A warm episode (from 788.4 to 786.1 ka), referred to a Bølling-Allerød-like event (Med-BA_{TIX}), followed the Med-H_{TIX} (Fig. 8) and was characterized by climate amelioration (alkenone-SST increase of 4 ℃, decrease of arctic-subarctic planktonic foraminifera, increase of dinocysts *S. mirabilis/hyperacanthus*; Maiorano et al., 2016) and distinct patterns of *Orbulina universa* and *Globorotalia inflata* (Marino et al., 2020). Upwards, a Younger Dryas-like episode (Med-YD_{TIX}) has been inferred based on a 2.5 ℃ decrease of alkenone-SST centered at 785.8 ka and on the short-term peaks of *Coccolithus pelagicus* ssp. *pelagicus*, *Neogloboquadrina pachyderma* (Fig. 8), and *Neogloboquadrina incompta*.

Following the Med-YD_{TIX} event, the SST records a quite sharp increase up to 16.5 ℃ at 785 ka marking the beginning of the climate optimum of MIS 19c and the increases in warm water taxa and coccolithophore productivity (Fig. 8). The ghost sapropel i-74 in early MIS 19c, from 785.0 ka to 782.6 ka (Fig. 8) and its internal variability have been described in previous papers to which we refer for details (Maiorano et al., 2016; Nomade et al., 2019; Marino et al., 2020). The climatic and stratigraphic value of the orbitally controlled sapropel i-74 represented a powerful tool for the chronological framework of the IS (Nomade et al., 2019). A lower oxygen content and stressed environmental conditions at the sea floor have been attested, within the $\delta^{13}C$ minimum (Fig. 8), by an increase in the benthic foraminiferal infauna/epifauna ratio (Stefanelli, 2003) and by a peak of the dinocyst *Polysphaeridium zoharyi* (Bertini et al., 2015; Maiorano et al., 2016) (star and diamond in figure 8) that similarly showed high abundance during sapropel deposition in MIS 5e (Giunta et al., 2006; Sangiorgi et al., 2006; Negri et al., 2015). The stable and stratified surface water conditions recognized during this sapropel were interrupted in the middle (at 783.5 ka) by a short-term increase in nutrients and mixing in sea surface water in agreement with the pattern of selected calcareous plankton taxa and the cooler and dryer conditions on land indicated by decrease of the mesothermic arboreal pollen taxa curve (see Marino et al., 2020). Such a sapropel interruption recalls the same mid-S1 interruption at ~8.2 ka in the Mediterranean Sea (Rohling et al., 1997; De Rijk et al., 1999; Rohling et al., 2015; Tesi et al., 2017; Filippidi and De Lange, 2019; Maiorano et al., 2019) related to a brief cooling event in the Northern Hemisphere (Rohling and Pälike, 2005), and chosen for the GSSP of the Northgrippian (Middle Holocene) in the NGRIP1 Greenland ice core (Walker et al., 2018). A short-term cooling in early MIS 19 has been also recorded in the central Italy Sulmona lacustrine section as evidence of freshwater discharges from residual ice-sheets, and compared to the Holocene 8.2 ka event (Regattieri et al., 2019). At all these data support the excellent climatostratigraphic record of wide-scale relevance archived in the IS and a potential similarity of climate instability between TIX and TI.

Higher abundances of calcareous plankton warm-water taxa, the occurrence of the tropical–subtropical mesopelagic teleostean fish *Bonapartia pedaliota* (Girone and Varola, 2001) during the maximum flooding at ~780 ka, together with higher alkenone-SST, higher productivity and increase in mesothermic arboreal pollen taxa are recorded during MIS 19c (Fig. 8). The warmer climate conditions (climate optimum) during MIS 19c lasted for ~11.5 ± 3.4 ky (Nomade et al., 2019) similarly to the full interglacial recorded in the lacustrine Sulmona section (i.e., 11 ky, Regattieri et al., 2019) or inferred in the North Atlantic records (i.e. 12.5–10.5 ky; Tzedakis et al., 2012; see also summary in Head, 2021). MIS 19c, however, was not a stable period due to variable conditions of sea level, dynamics of NIG and climate (Marino et al., 2020). The evidence comes from three main warmer and wetter phases within about 11 kyr in both marine and continental settings (I, II and III in Fig. 8). These three warmer phases have been compared to those recognized on the Iberian Margin (Sánchez-Goñi et al., 2016) and linked to both oceanographic and atmospheric processes. Higher-frequency variability has been also indicated by the abundance pattern of the planktonic foraminifer *Trilobatus sacculifer* that shows multiple oscillations related to variable conditions in seasonality and humidity (Marino et al., 2020).

The end of substage MIS 19c, starting from ~774 ka, is marked by the $\delta^{18}O$ record, alkenone-SST drop, and concurrent decrease of Mesothermic Arboreal Pollen Taxa, as well as by the patterns of calcareous plankton key taxa (Fig. 8). These patterns describe MIS 19b that is interpreted as the first seesaw bipolar oscillation (Nomade et al., 2019). The prominent drop of 8–9 ℃ in the alkenone-SST, with a minimum of 12.1 ℃ at 772.8 ka, has been associated with possible continental cold and dry air flux by enhanced Siberia High pressure into the central Mediterranean (Marino et al., 2020). The duration of the cold MIS 19b (~1.2 kyr) at the IS, when compared with several worldwide paleoclimatic records, is included between 775.0 and 772.5 ka (Fig. 9 in Nomade et al., 2019), after the insolation minimum. The MIS 19b short duration at the IS is consistent with the 800–1000 kyr duration at the Pianico-Sellere paleolake located in North Italy based on the pollen record (Moscariello et al., 2000; Rossi, 2003; Mangili et al., 2007) (Fig. 8 in Nomade et al., 2019), and is a distinctive climatostratigraphic event synchronous with the first IRD occurrence after the full interglacial MIS 19c in northern Atlantic (Kleiven et al., 2011), and very close to the Ar/Ar dated V4 and $^{10}Be/^{9}Be$ peak.

The stadial-interstadial oscillations outlined by the $\delta^{18}O$ record in MIS 19a coherently parallel the patterns of calcareous plankton and mesothermic arboreal pollen taxa as well as alkenone-SST. The $\delta^{13}C$ fluctuations are the response to more (higher $\delta^{13}C$ values) or less (lower $\delta^{13}C$ values) ventilated and oxygenated bottom water during respectively lower or higher paleodepth in the basin (Fig. 5). This oscillatory climatic regime may have been increased by cyclic north-

wards shifts of the Intertropical Convergence Zone (ITCZ) over the Mediterranean region during the precession minimum perhaps creating a zonal teleconnection between the Asian summer Monsoon and the Mediterranean climate (Nomade et al., 2019). At the IS the high amplitude oscillations of stadials and interstadials in MIS 19a may have been also amplified by local phenomena such as different amounts of fresh water from the neighboring land. The wetter/higher winter precipitation and warmer condition during interstadials, and the drier and cold condition during stadials are clearly shown by changes in pollen assemblages (Bertini et al., 2015), coccolithophore productivity (Maiorano et al., 2021), mineralogical/grain size variations (Maiorano et al., 2016), and by light-dark sediment color patterns in the IS (Fig. 5).

A cooling trend at the top of the IS up to the MIS 18 glacial onset at 757 ka is observed and is sustained by the heavier values of $\delta^{18}O$ together with the increased abundance of the cold-water taxa *C. pelagicus* ssp. *pelagicus* and *N. pachyderma* along with a decreasing trend of alkenone-SST, warm water taxa, and coccolithophore productivity (Fig. 8) (Bertini et al., 2015; Maiorano et al., 2016, 2021; Nomade et al., 2019; Marino et al., 2020).

Comparison of Ideale Section to the Chiba Composite Section

The correlation of IS to the composite section of Chiba (CcS) is shown in figures 9 and 10. The CcS is an expanded marine sedimentary succession (~ 90 m thick) crossing the MIS 20–MIS 18 interval. It has been studied and described in several published articles (e.g., Kazaoka et al., 2015; Suganuma et al., 2015, 2018; Nishida et al., 2016; Takeshida et al., 2016; Okada et al., 2017; Simon et al., 2019; Haneda et al., 2020 a, b; Kameo et al., 2020; Balota et al., 2021; Izumi et al., 2021; Kubota et al., 2021) including the summary of Head (2021). The GSSP of Chibanian Stage is positioned 1.1 m below the directional midpoint of the MBB (773.1 ka, Okada et al., 2017; astronomical age 772.9 ka, Suganuma et al., 2021), at the base the Ontake-Byakubi-E tephra bed (Byk-E, U-Pb age of 772.7 ± 7.2 ka, Suganuma et al., 2015; astronomical estimated age of 774.1 ka, Suganuma et al., 2021) in the 17.7 m thick Chiba section (Suganuma et al., 2021, and references therein) (Fig. 9). The GSSP occurs immediately below the top of Marine Isotope Substage 19c.

The depositional environment of the IS was able to record global sea level and climate changes, and was influenced by both freshwater and terrigenous/nutrient input of terrestrial origin related to the proximity to Italian coasts, as well as by the variable influx of Modified Atlantic waters or Atlantic meltwaters through the Gibraltar Strait into the Ionian Sea during changeable North Atlantic ice sheet and AMOC dynamics (Maiorano et al., 2016, 2021; Nomade et al., 2019; Marino et al., 2020).

Despite the two sections being located in different areas and paleogeographic-paleoenvironmental settings, a clear correlation can be seen between them. The IS, like the CcS, encompasses the MIS 20–MIS 19 interval and shows several benthic $\delta^{13}C$ and $\delta^{18}O$ oscillations driven by global and regional paleoenvironmental variations. The isotopic oscillations compare well between the IS and CcS and have been correlated to worldwide marine and continental records (e.g., Nomade et al., 2019; Marino et al., 2020; Suganuma et al., 2021; Head, 2021). In the CcS, millennial-scale climate variability during Termination IX has been recognized: a Younger Dryas-type cooling event has been indicated based on the brief reduction in surface and subsurface temperatures (DT in Haneda et al., 2020b) associated with the radiolarian sea-surface temperature index (Tr ratio in Suganuma et al., 2021). In the IS, based on multiple proxies, the climate instability recorded during TIX is more detailed and consists of the brief episodes named Med-H_{TIX}, Med-BA_{TIX}, and Med-YD_{TIX}, and associated with the analogous Heinrich, Bølling-Allerød, and Younger-Dryas events that occurred during Termination I (Maiorano et al., 2016; Marino et al., 2020).

The duration of the full interglacial, approximating MIS 19c, compares well between the sections being of 9.9 kyr duration (785.0 to 775.1 ± 5 ka) at the CcS (Haneda et al., 2020b) and of 11.5 ± 3.4 ka at the IS (Nomade et al., 2019) (Table 2).

From a chronological point of view, the excellent $^{10}Be/^{9}Be$ record in the IS is relevant: a near doubling of the $^{10}Be/^{9}Be$ ratio, as a result of low geomagnetic dipole moments at the Matuyama–Brunhes boundary interval, occurs through the MIS 19c–MIS 19b transition, as in the CcS. There, the higher values of the ratio are recorded in the latest MIS 19c corresponding to the MBB recorded by the virtual geomagnetic pole and relative paleointensity data. The near doubling of the $^{10}Be/^{9}Be$ ratio, dated between 776.35 ka and 771.87 ka in the IS (Nomade et al., 2019), significantly includes the volcaniclastic layer V4 Ar/Ar dated at 774.1 ± 0.9 ka, which, remarkably, is the same age as the Chibanian GSSP (Fig. 9).

A robust correlation exists between the CcS and IS sections through the MIS 19a interval based on millennial-scale stadial–interstadial oscillations in the isotope records. The interstadials i1-i4 in MIS 19a at the CcS (Head, 2021) and 19a1–19a3 at the IS (Nomade et al., 2019) (Fig. 9) have comparable durations and are linked to northwards displacements of the Kuroshio Current Front at CcS (Haneda et al., 2020b) and to climatically induced sea surface water warming and wetter conditions on land as well as to local seawater freshening at the IS (Nomade et al., 2019; Maiorano et al., 2016, 2021; Marino et al., 2020).

The distributions through time of the main marine and terrestrial key fossils described in both sections and useful for their comparison are significant for climatostratigraphy (Fig. 10) and sustain the climate variability recorded in the isotope curves, thus representing additional and notable proxies to correlate the far distant IS and CcS. The cold and warm water calcareous plankton taxa (foraminifera and nannofossils) exhibit similar patterns between the two sections at the least at orbital scale, highlighting cold and warm conditions in surface waters during glacial and interglacial phases, respectively. A more distinct matching between calcareous plankton patterns and isotope records and alkenone-SST is observed at the IS (Fig. 10). No biozonal events are recorded in either section through MIS 20–MIS 18; however, the absence of *Gephyrocapsa* ≥ 5 μm in MIS 19a in the CcS (Kameo et al., 2020; Suganuma et al., 2021) has been correlated to the second temporary disappearance of *Gephyrocapsa omega* (td2 in Maiorano and Marino, 2004) in the IS where the species reappears at 766 ka (in MIS 19a-2) (Table 1, Fig. 10). The pollen assemblages recorded in the two sections, although diverse due to the different floristic composition and main vegetation structural features between the Mediterranean and east-central Japanese archipelago areas, show similarities in terms of regional responses to global climate change. The Chiba pollen record

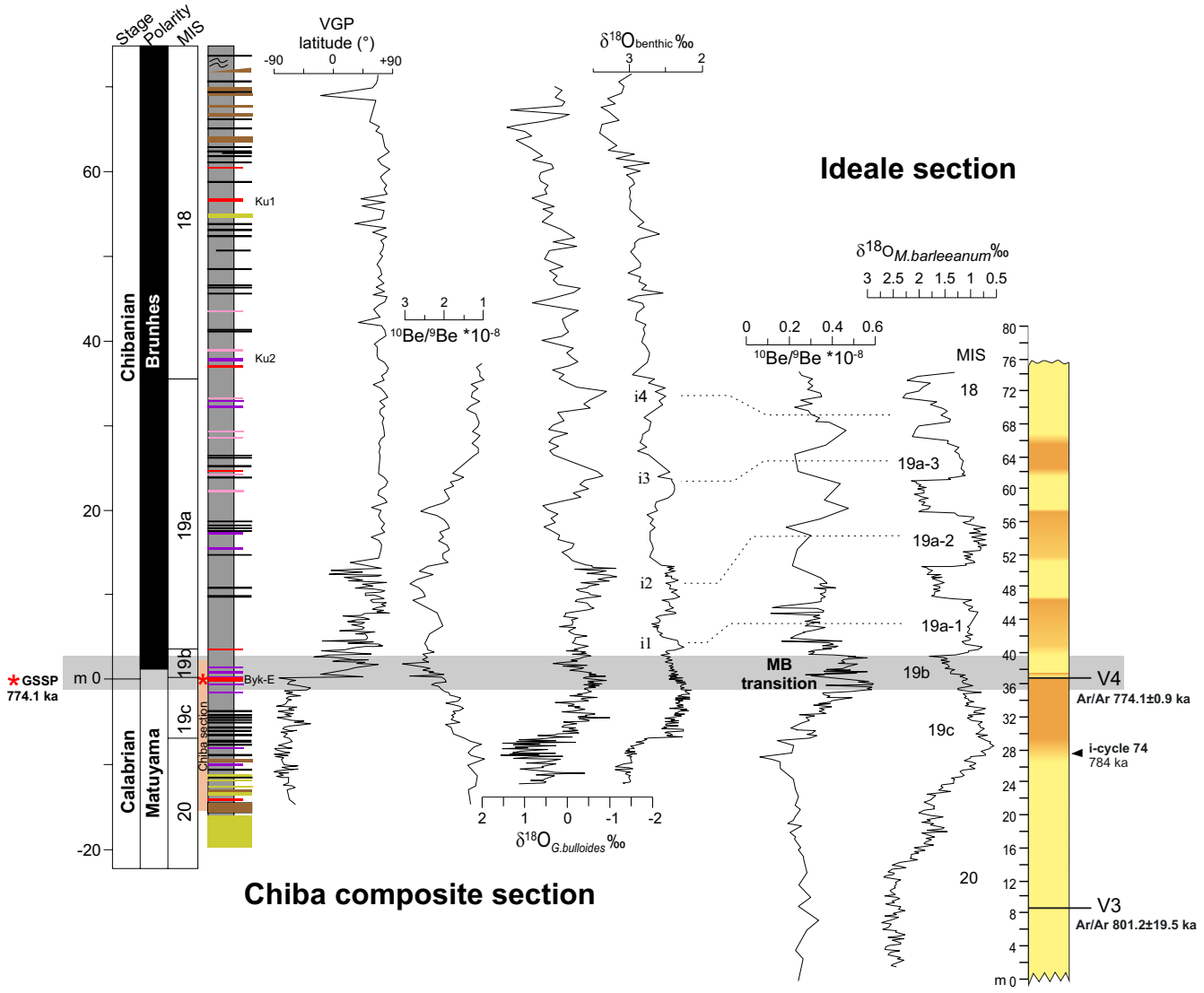

Figure 9. Comparison of the main chronological and stratigraphic data between the Chiba composite section (from Suganuma et al., 2021, cum reference therein) and the Ideale section (mainly from Nomade et al., 2019, see reference therein). i1–i4 are the interstadials in MIS 19a based on Haneda et al. (2020b) and Head (2021), and dashed lines mark their correlation with homologous interstadials 19a1–a3 in the isotope record at the Ideale section. Grey band crossing the dataset of the two sections highlights the primary correlation at the level of Chibanian GSSP (see text for detail) and the GSSP boundary interval proposed in the Ideale section. Note that the scale of the $^{10}Be/^{9}Be$ record is reversed between the two sections.

reflects regional vegetational changes in the eastern to northern parts of the Japanese archipelago, based on the present-day vegetational distribution of natural forest communities (Suganuma et al., 2018). The ratio of broadleaved tree pollen to the total arboreal pollen (broadleaved/AP) at the CcS significantly increases during MIS 19c, while boreal coniferous trees decrease, reflecting a warm period. Dinocyst assemblages from the CcS reveal the end of MIS 19c with a sharp increase in *Protoceratium reticulatum* resulting from the influence of cooler, mixed, nutrient-rich waters of the Kuroshio-Oyashio Interfrontal Zone and linked to a southward shift of the Kuroshio Extension (Balota et al., 2021). At the IS, the increase/decrease in Mesothermic Arboreal Pollen Taxa, a proxy for warmer and wetter conditions, distinctly follows the interglacial–glacial and interstadial–stadial cycles, respectively (Fig. 10), in considerable agreement with alkenone-SST and $\delta^{18}O$ patterns, especially during MIS 19b-a. Moreover, an expansion of steppe vegetation on land is recorded in the IS during glacial and stadial phases (Bertini et al., 2015; Maiorano et al., 2016).

Requirements Fulfilled by the Ideale Section as a SABS for the Middle Pleistocene GSSP

The IS is one of the most detailed and continuous sedimentary record of the Lower–Middle Pleistocene transition. The plethora of chronostratigraphic features and comprehensive paleoclimate history available at the IS strongly makes it an excellent SABS for the Lower–Middle Pleistocene Substage and Chibanian GSSP. The GSSP boundary interval in the IS is well represented by the sedimentary interval

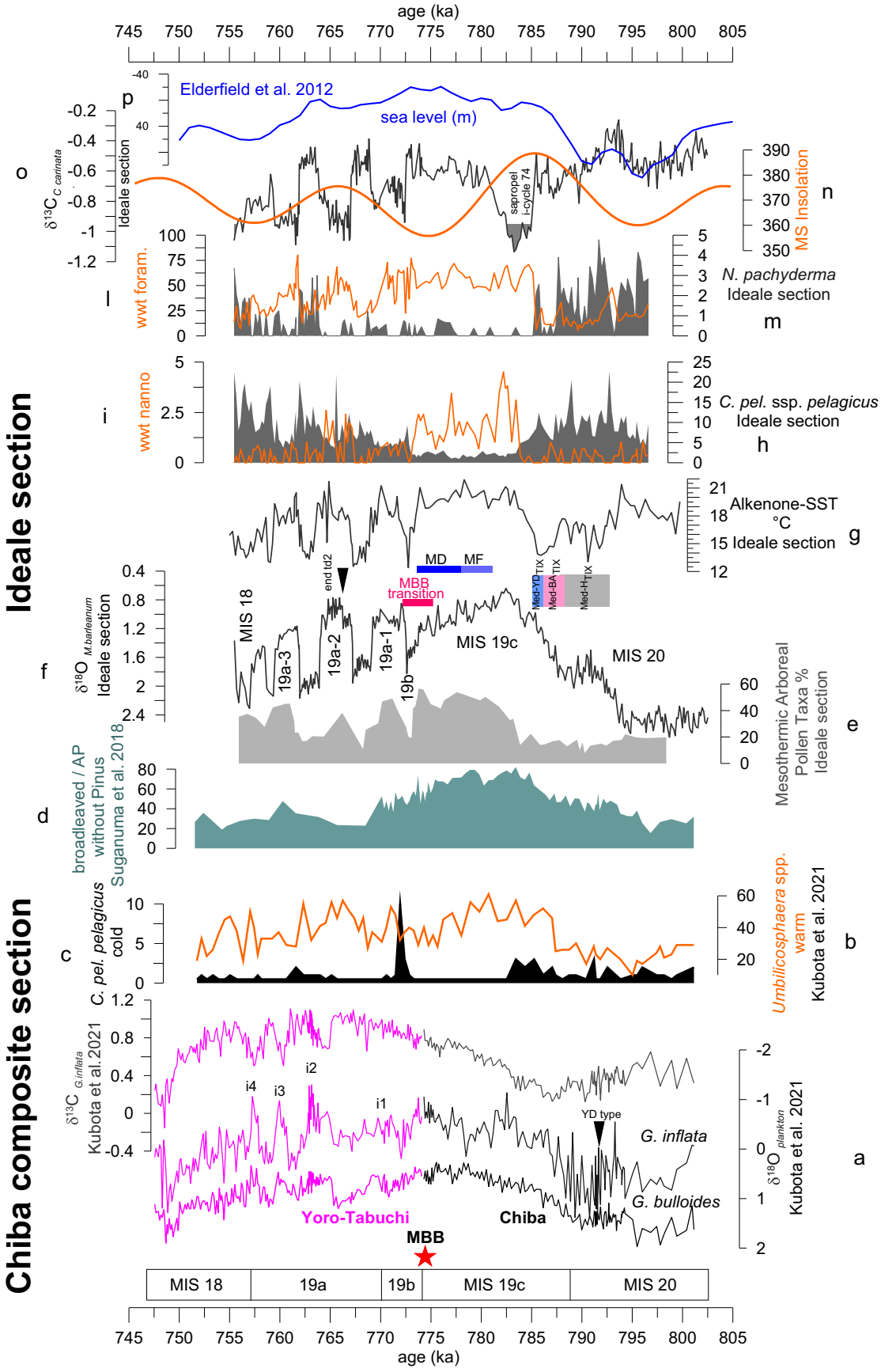

Figure 10. Correlation of main climatostratigraphic proxies between the Chiba composite section (a–d) and the Ideale section (e–o). (o): Mean Summer Insolation 65°N is from Laskar et al. (2004). (p): sea-level curve from Elderfield et al. (2012). i1–i4 on $\delta^{18}O_{Gb\,ulloides}$ from the Chiba composite section are interstadials in MIS 19a based on Haneda et al. (2020b) and Head (2021) (see text for detail).

from 35.50 to 39.50 m, which corresponds to the interval of the highest values of the $^{10}Be/^{9}Be$ ratio (from ~776.35 to 771.87 ka) and includes the V4 tephra ($^{40}Ar/^{39}Ar$ age of 774.1±0.9 ka) and the MIS 19c–MIS 19b transition (Figs. 7–9).

The IS wholly satisfies the requirements for the SABS (Head et al., 2023b).

The following requirements are fulfilled:

1. Adequate exposure and thickness of 74 m representing the MIS 20–18 interval, as part of the more extended, astronomically calibrated Montalbano Jonico section encompassing MIS 37 to early MIS 16;

2. Continuous sedimentation varying from circalittoral to upper bathyal facies, without hiatuses or turbiditic levels and without metamorphic phenomena;

3. High sedimentation rate useful for high-resolution analyses (90–200 cm/kyr);

4. Abundance and diversity of fossils (calcareous nannofossils, planktonic and benthic foraminifera, pollen, ostracods, dinocysts, molluscs, echinoids, crabs, otoliths, rare deep-sea corals) useful for paleoenvironmental reconstructions;

5. Radiometric dating of tephra layers V3 and V4, the latter with an age of 774.1±0.9 ka identical to that of the Chibanian GSSP;

6. Very high resolution (~90–200 years) of oxygen and carbon isotopes (*Melonis barleeanum* and *Cassidulina carinata*) and of the authigenic $^{10}Be/^{9}Be$ ratio; low-resolution data of planktonic $\delta^{18}O$ is also available.

7. Prominent peak of the $^{10}Be/^{9}Be$ ratio at the MIS 19c–MIS 19b transition, marking the Matuyama–Brunhes transition;

8. Very high-resolution paleoclimate reconstruction based on calcareous plankton and pollen assemblages, and alkenone-derived SST;

9. Archive of detailed climate evolution at orbital-suborbital up to millennial scale of the mid-Pleistocene transition including an excellent record of Termination IX and oscillations in MIS 19a of worldwide significance;

10. Location in the Special Natural Reserve of Montalbano Jonico badlands precluding any kind of banned urban development;

11. Excellent accessibility, being about 1 km from the state road SS598 from which the IS can be reached by a short (30 minutes) walk on an easy path or by means a vehicle (10 minutes).

12. Sample collection in the Special Natural Reserve of Montalbano Jonico badlands is possible under permission of Matera Provincial Administration.

Acknowledgements

The authors thank the numerous students that worked on the badland of Montalbano Jonico for their bachelor/master and PhD theses, and all the scientists that contributed to the research in this area, among them: A. D'Alessandro, L. Sagnotti and his team, D.L. Bourlès and ASTER Team, D. Barra, G. Aiello, L. Sabato, F. Lirer, L. Capotondi, P. Di Leo, S. Joannin, S. Stefanelli, M. Brilli. The authors espress gratitude to all the Mayors and government of Montalbano Jonico town for their readiness in favoring the work in the field during the years. The support of J. Zalasiewicz and colleagues of the Subcommission on Quaternary Stratigraphy, and the encouragement of M. Head are greatly appreciated. A special gratitude is esppressed to Neri Ciaranfi for his enthusiastic role in leading and encouraging the scientific research on the Montalbano Jonico badlands for many years.

References

Aguirre, E., and Pasini, G., 1985, The Pliocene–Pleistocene Boundary. Episodes, v. 8, pp. 116–120.

Aiello, G., Barra, D., and Parisi, R., 2015, Lower–Middle Pleistocene ostracod assemblages from the Montalbano Jonico section (Basilicata, southern Italy). Quaternary International, v. 383, pp. 47–73. doi:10.1016/j.quaint.2014.11.010

Azzaroli, A., Perno, U., and Radina, B., 1968, Note illustrative della Carta Geologica d'Italia alla scala 1:100.000, Foglio 188 Gravina di Puglia. Servizio Geologico Italiano, 57 p.

Azzarone, M., Ferretti, P., Rossi, V., Scarponi, D., Capraro, L., Macrì, P., Huntley, J.W., and Faranda, C., 2018, Early–middle Pleistocene benthic turnover and oxygen isotope stratigraphy from the central Mediterranean (Valle di Manche, Crotone Basin, Italy): data and trends. Data Brief, v.17, pp. 1099–1107. doi:10.1016/j.dib.2018.02.017

Backman, J., Raffi, I., Rio, D., Fornaciari, E., and Pälike, H., 2012, Biozonation and biochronology of Miocene through Pleistocene calcareous nannofossils from low and middle latitudes. Newsletters on Stratigraphy, v. 45, pp. 221–244. doi:10.1127/0078-0421/2012/0022

Balota, E.J., Head, M.J., Okada, M., Suganuma, Y., and Haneda, Y., 2021, Paleoceanography and dinoflagellate cyst stratigraphy across the Lower–Middle Pleistocene Subseries (Calabrian–Chibanian Stage) boundaryat the Chiba composite section, Japan. Progress in Earth and Planetary Science, v. 8, pp. 48. doi:10.1186/s40645-021-00438-3

Barker, S., Knorr, G., Edwards, R.L., Rarrenin, F., Putnam, A.E., Skinner, L.C., Wolff, E., and Ziegler, M., 2011, 800,000 years of abrupt climate variability. Science, v. 334, pp. 347–351.

Bassinot, F., Labeyrie, L., Vincent, E., Quidelleur, X., Shackleton, N. and Lancelot, Y., 1994, The astronomical theory of climate and the age of the Brunhes–Matuyama magnetic reversal. Earth Planetary Science Letter, v. 126, pp. 91–108. doi:10.1016/012-821X(94)90244-5

Batistić, M., Viličić, D., Kovačević, V., Jasprica, N., Lavignec, H., Carića, M., Garić, R., Cara, A., 2017. Winter phytoplankton blooms in the offshore south Adriatic waters (1995–2012) regulated by hydroclimatic events: Special emphasis on the exceptional bloom of 1995. Biogeoscience Discussion, doi:10.5194/bg-2017-205

Béthoux, J. P., Morin, P., Chaumery, C., Connan, O., Gentili, B., and Ruiz-Pino, D., 1998, Nutrients in the Mediterranean Sea, mass balance and statistical analysis of concentrations with respect to environmental change. Marine Chemistry, v. 63, pp. 155–169. doi:10.1016/S0304-4203(98)00059-0

Bertini, A., Toti, F., Marino, M., and Ciaranfi, N., 2015, Vegetation and climate across the Early–Middle Pleistocene transition at the Montalbano Jonico section (southern Italy). Quaternary International, v. 383, pp. 74–88. doi:10.1016/j.quaint.2015.01.003

Bickert, T., Curry, W.B., and Wefer, G., 1997, Late Pliocene to Holocene (2.6–0 Ma) western equatorial Atlantic deep-water circulation: inferences from benthic stable isotope, in Shackleton, N.J., Curry, W.B., Richter, C., and Bralower, T.J., eds., Proceedings of the Ocean Drilling Program: Scientific Results, v. 154, College Station (TX), pp. 239–253.

Bignami, F., Sciarra, R., Carniel, S., and Santoleri, R., 2007, Variability of Adriatic Sea coastal turbid waters from SeaWiFS imagery. Journal of Geophysical Research, v. 112, C03S10.

Boenzi, F., Capolongo, D., Gallicchio, S., and Di Pinto, G., 2014, Morphostructure of the Lucania Apennines front between the Basento and Salandrella rivers (Southern Italy). Journal of Maps, v. 10, pp. 478–486. doi:10.1080/17445647.2014.888017

Bonardi, G., D'Argenio, B., Di Nocera, S., Marsella, E., Pappone, G., Pescatore, T.S.S., Senatore, M.R., Sgrosso, I., Ciaranfi, N., Pieri, P., and

Ricchetti, G., 1988, Carta geologica dell'Appennino meridionale. 74° Congresso Società Geologica Italiana, Carta geologica in scala 1: 250.000.

Brilli, M., 1998. Stratigrafia isotopica del carbonio e dell'ossigeno della successione infra e mesopliocenica di Montalbano Jonico (Basilicata, Italia meridionale). Unpublished PhD thesis. Università degli Studi di Roma "La Sapienza", 112 p.

Brilli, M., Lerche, J., Ciaranfi, N., and Turi, B., 2000, Evidence of precession and obliquity orbital forcing in Oxygen 18 isotope composition of Montalbano Jonico section (Basilicata, southern Italy). Applied Radiation and Isotope, v. 52, pp. 957–964.

Capraro, L., Maiorano, P., 2023, Italian GSSPs of the Quaternary System. Alpine and Mediterranean Quaternary, v. 36, pp. 1–23, doi:10.26382/AMQ.2023.02

Capraro L., Asioli A., Backman J., Bertoldi R., Channell J.E.T., Massari F., and Rio D., 2005, Climatic patterns revealed by pollen and oxygen isotope records across the Matuyama/Brunhes Boundary in central Mediterranean (Southern Italy). Geological Society of London, Spec. Publ., v. 247, pp. 159–182.

Capraro, L., Massari, F., Rio, D., Fornaciari, E., Backman, J., Channell, J. E. T., Macrì, P., Prosser, G., and Speranza, F., 2011, Chronology of the lower–middle Pleistocene succession of the south-western part of the Crotone Basin (Calabria, southern Italy). Quaternary Science Reviews, v. 30, pp. 1185–1200.

Capraro, L., Ferretti, P., Macrì, P., Scarponi, D., Tateo, F., Fornaciari, E., Bellini, G., and Dalan, G., 2017, The Valle di Manche section (Calabria, Southern Italy): A high resolution record of the Early–Middle Pleistocene transition (MIS 21–MIS 19) in the Central Mediterranean. Quaternary Science Reviews, v. 165, pp. 31–48.

Capraro, L., Tateo, F., Ferretti, P., Fornaciari, E., Macrì, P., Scarponi, D., Preto, N., Xian, F., Kong, X., and Xie, X., 2019, A Mediterranean perspective on 10Be, sedimentation and climate around the Matuyama/Brunhes boundary: les liaisons dangereuses? Quaternary Science Reviews, v. 226.106039.

Caron, B., Siani, G., Sulpizio, R., Zanchetta, G., Paterne, M., Santacroce, R., Terna, E., and Zanella, E., 2012, Late Pleistocene to Holocene tephrostratigraphic record from the Northern Ionian Sea. Marine Geololgy, v. 311, pp. 41–51.

Casnedi R., 1988, La Fossa bradanica: origine, sedimentazione e migrazione. Memorie Società Geologica Italiana, v. 41, pp. 439–448.

Ceregato, A., Raffi, S., and Scarponi, D., 2007, The circalittoral/bathyal in the Middle Pliocene of Northern Italy: the case of the Korobkovia oblonga–Jupiteria concave paleocommunity type. Geobios, v. 40, pp. 555–572.

Channell, J.E.T., Hodell, D.A., Xuan, C., Mazaud, A., and Stoner, J.S., 2008, Age calibrated relative paleointensity for the last 1.5Myr at IODP Site U1308 (North Atlantic). Earth Planetary Science Letters, v. 274, pp. 59–71.

Channell, J.E.T., Xuan, C., and Hodell, D.A., 2009, Stacking paleointensity and oxygen iso-tope data for the last 1.5 Myr (PISO-1500). Earth Planetary Science Letters, v. 283, n. 1–4, pp. 14–23. doi:10.1016/j.epsl.2009.03.012

Channell, J.E.T, 2017, Complexity in Matuyama–Brunhes polarity transitions from North Atlantic IODP/ODP deep-sea sites. Earth and Planetary Science Letters, v. 467, pp. 43–56.

Channell, J.E.T., Hodell, D.A., Singer, B.S., and Xuan, C., 2010, Reconciling astrochronological and 40Ar/39Ar ages for the Matuyama–Brunhes boundary in the late Matuyama Chron. Geochemistry, Geophysics, Geosystems, v. 11, Q0AA12, doi:10.1029/2010GC003203

Ciaranfi, N., Marino, M., Sabato, L., D'Alessandro, A., and De Rosa, R., 1996, Studio geologico stratigrafico di una successione infra e mesopleistocenica nella parte sudoccidentale della Fossa Bradanica (Montalbano Jonico, Basilicata): Bollettino della Società Geologica Italiana, v. 15, pp. 379–391.

Ciaranfi, N., D'Alessandro, A., 2005, Overview of the Montalbano Jonico area and section: a proposal for a boundary stratotype for the lower–middle Pleistocene, southern Italy Foredeep. Quaternary International., v 131, pp. 5–10.

Ciaranfi, N., D'Alessandro, A., Girone, A., Maiorano, P., Marino, M., Soldani, D., and Stefanelli, S., 2001, Pleistocene sections in the Montalbano Jonico area and the potential GSSP for Early–Middle Pleistocene in the Lucania Basin (southern Italy). Memorie di Scienze Geologiche, v. 53, pp. 67–83.

Ciaranfi, N., D'Alessandro, A., and Marino, M., 1997, A candidate section for the lower–middle Pleistocene boundary (Apennine foredeep, South Italy). In: Naiwen W., Remane J. (Eds.), Proceedings 30th International Geological Congress. v. 11, pp. 201–211.

Ciaranfi, N., D'Alessandro, A., Marino, M., and Sabato, L., 1994, The Montalbano Jonico Section in the Bradanic Foredeep (southern Italy): a potential early–middle Pleistocene Boundary Stratotype. Contribution in Cita, M.B., and Castradori, D., 1994, Workshop on marine sections from the Gulf of Taranto (Southern Italy) usable as potential stratotypes for the GSSP of the Lower, Middle and Upper Pleistocene (Bari, Italy, sept. 29– oct. 4, 1994). Il Quaternario, v. 7, pp. 677–692.

Ciaranfi, N., Lirer, F., Lirer, L., Lourens, L.J., Maiorano, P., Marino, M., Petrosino, P., Sprovieri, M., Stefanelli, S., Brilli, M., Girone, A., Joannin, S., Pelosi, N., and Vallefuoco, M., 2010, Integrated stratigraphy and astronomical tuning of the Lower–Middle Pleistocene Montalbano Jonico land section (southern Italy). Quaternary International, v. 210, pp. 109–120.

Ciaranfi, N., Head, M.J., and Marino, M., 2015, Report of the Field Workshop on the Lower–Middle Pleistocene transition in Italy. Quaternary Perspectives, v. 22, pp. 12–14

Cilumbriello, A., Tropeano, M., and Sabato, L., 2008, The Quaternary terraced marine deposits of the Metaponto area (Southern Italy) in a sequence stratigraphic perspective. In: A. Amorosi, B. U. Haq, and L. Sabato (Eds.), Advances in application of sequence stratigraphy in Italy, v. 1, pp. 27–54. GeoActa, Special Publication.

Cita, M.B., Capraro, L., Ciaranfi, N., Di Stefano, E., Lirer, F., Maiorano, P., Marino, M., Raffi, I., Rio, D., Sprovieri, R., Stefanelli, S., and Vai, G.B., 2008, The Calabrian Stage redefined. Episodes, v. 31, pp. 408–419.

Cita, M.B., Gibbard, P.L., Head, M.J., and The Subcommission on Quaternary Stratigraphy, 2012, Formal ratification of the GSSP for the base of the Calabrian Stage (second stage of the Pleistocene Series, Quaternary System). Episodes, v. 35, pp. 388–397.

Civitarese, G., Gačič, M., Lipizer, M., and Eusebi Borzelli, G.L., 2010, On the impact of the Bimodal Oscillating System (BiOS) on the biogeochemistry and biology of the Adriatic and Ionian Seas (Eastern Mediterranean). Biogeosciences, v. 7, pp. 3987–3997.

Cohen, K.M., Finney, S.C., Gibbard, P.L., and Fn J.X., 2013, The ICS International Chronostratigraphic Chart. Episodes, v. 36, pp. 200–204.

D'Alessandro, A., La Perna, R., and Ciaranfi, N., 2003, Response of macrobenthos to changes in paleoenvironment in the Lower–Middle Pleistocene (Lucania Basin, southern Italy). Il Quaternario, v. 16, pp. 167–182.

De Rijk, S., Troelstra, S.R., and Rohling, E.J., 1999, Benthic foraminiferal distribution in the Mediterranean Sea. Journal Foraminifera Research, v. 29, pp. 93–103.

Doglioni, C., Tropeano, M., Mongelli, F., and Pieri, P., 1996, Middle–Late Pleistocene uplift of Puglia: an "anomaly" in the Apenninic foreland. Memorie Società Geologica Italiana, v. 51, pp. 101–117.

D'Ortenzio, F., Ribera d'Alcalà, M., 2009, On the trophic regimes of the Mediterranean Sea: A satellite analysis. Biogeosciences, v. 6, pp. 139–148, doi:10.5194/bg-6-139

Dreyfus, G.B., Raisbeck, G.M., Parrenin, F., Jouzel, J., Guyodo, Y., Nomade, S., and Mazaud A., 2008, An ice core perspective on the age of the Matuyama–Brunhes boundary. Earth and Planetary Science Letters, v. 274, pp.151–156.

Elderfield, H., Ferretti, P., Greaves, M., Crowhurst, S., McCave, I.N.,

Hodell, D., and Piotrowski, A.M., 2012, Evolution of ocean temperature and ice volume through the mid-Pleistocene climate transition. Science, v. 337, pp. 704–709.

Emeis, K., Sakamoto, T., Wehausen, R., and Brumsack, H.J., 2000, The sapropel record of the eastern Mediterranean Sea - results of Ocean Drilling Program Leg 160. Palaeogeography, Palaeoclimatology, Palaeoecology, v. 158, pp. 371–395.

Ferretti, P., Crowhurst, S.J., Naafs, B.D.A., and Barbante, C., 2015, The Marine Isotope Stage 19 in the mid-latitude North Atlantic Ocean: astronomical signature and intra-interglacial variability. Quaternary Science Reviews, v. 108, pp. 95–110.

Filippidi, A., De Lange, G.J., 2019, Eastern Mediterranean deep water formation during Sapropel S1: a reconstruction using geochemical records along a bathymetric transect in the Adriatic outflow region. Paleoceanography and Paleoclimatology, v. 34, pp. 409–429. doi:10.1029/2018PA003459

Gačić, M., Eusebi Borzelli, G.L., Civitarese, G., Cardin, V., and Yari, S., 2010, Can internal processes sustain reversals of the ocean upper circulation? The Ionian Sea example. Gephysical Research Letters, v. 37, L09608. doi:10.1029/2010GL043216

Gallicchio, S., Colacicco, R., Capolongo, D., Girone, A., Maiorano, P., Marino, M., and Ciaranfi, N., 2023, Geological features of the Special Nature Reserve of Montalbano Jonico Badlands (Basilicata, Southern Italy), Journal of Maps, doi:10.1080/17445647.2023.2179435

Giaccio, B., Castorina, F., Nomade, S., Scardia, G., Voltaggio, M., and Sagnotti, L., 2013, Revised chronology of the Sulmona lacustrine succession, central Italy; Journal of Quaternary Science, v. 28, pp. 545–55.

Giaccio, B., Regattieri, E., Zanchetta, G., Nomade, S., Renne, P.R., Sprain, C.J, Drysdale, R.N., Tzedakis, P.C., Messina, P., Scardia, G., Sposato, A., and Bassinot, F., 2015, Duration and dynamics of the best orbital analogue to the present interglacial. Geology, doi:10.1130/G36677.1

Giaccio, B., Zanchetta, G., with the collaboration of Galli, P., Nomade, S., Regattieri, E., Sagnotti., L., 2023, The Quaternary evolution of Sulmona Basin, central Italy. Proposed excursion for INQUA Congress 2023, Rome. https://inquaroma2023.org/wp-content/uploads/2022/10/5-Post.pdf.

Gibbard, P.L., Head, M.J., Walker, M.J.C., and the Subcommission on Quaternary Stratigraphy, 2010, Formal ratification of the Quaternary System/Period and the Pleistocene Series/Epoch with a base at 2.58 Ma. Journal of Quaternary Science, v. 25, pp. 96–102.

Girone, A., 2005, Response of otolith assemblages to sea-level fluctuations at the Lower Pleistocene Montalbano Jonico section (southern Italy). Bollettino della Società Paleontologica Italiana, v. 44, pp. 35–45.

Girone, A., and Varola, A., 2001, Fish otoliths from the Middle Pleistocene deposits of Montalbano Jonico (southern Italy). Bollettino Società Paleontologica Italiana, v. 40, pp.431–443.

Girone, A., Capotondi, L., Ciaranfi, N., Di Leo, P., Lirer, F., Maiorano, P., Marino, M., Pelosi, N., and Pulice, I., 2013, Paleoenvironmental change at the lower Pleistocene Montalbano Jonico section (southern Italy): global versus regional signals. Palaeogeography, Palaeoclimatology, Palaeoecology, v. 371, pp. 62–79.

Giunta, S., Negri, A., Maffioli, P., Sangiorgi, F., Capotondi, L., Morigi, C., Principato, M.S., and Corselli, C., 2006, Phytoplankton dynamics in the eastern Mediterranean Sea during marine isotopic stage 5e. Palaeogeography, Palaeoclimatology, Palaeoecology, v. 235, pp. 28–47.

Goudeau, M.L.S., Grauel, A.L., Bernasconi, S.M., and de Lange, G.J., 2013, Provenance of surface sediments along the southeastern Adriatic coast off Italy: an overview. Estuarine, Coastal and Shelf Science, v. 134, pp. 45–56.

Grauel, A. L., Goudeau, M. L., de Lange, G. J., and Bernasconi, S. M., 2013, Climate of the past 2500 years in the Gulf of Taranto, central Mediterranean Sea: A high-resolution climate reconstruction based on $\delta^{18}O$ and $\delta^{13}C$ of Globigerinoides ruber (white). The Holocene, v. 23, pp. 1440–1446, doi:10.1177/0959683613493937

Haneda, Y., Okada, M., Suganuama, Y., and Kitamura, T., 2020a, A full sequence of the Matuyama–Brunhes geomagnetic reversal in the Chiba composite section, central Japan. Progress in Earth and Planetary Science, v. 7, 44 p. doi:10.1186/s40645-020-00354-ydoi:10.1016/j.epsl.2019.115936

Haneda, Y., Okada, M., Kubota, Y., and Suganuama, Y., 2020b, Millennial-scale hydrographic changes in the northwestern Pacific during marine isotope stage 19: teleconnections with ice melt in the North Atlantic. Earth and Planetary Science Letters, v. 531, 115936.

Head, M.J., Pillans, B., and Farquhar, S.A., 2008, The Early–Middle Pleistocene transition: characterization and proposed guide for the defining boundary. Episodes, v. 31, pp. 255–259.

Head, M.J., 2019, Formal subdivision of the Quaternary System/Period: present status and future directions. Quaternary International, v. 500, pp. 32–51.

Head, M.J., 2021, Review of the Early–Middle Pleistocene boundary and Marine Isotope Stage 19. Progress in Earth and Planetary Science. doi:10.1186/s40645-021-00439-2

Head, M.J., Pillans, B., Zalasiewicz, J.A., and ICS Subcommission on Quaternary Stratigraphy, 2021. Formal ratification of subseries/subepochs for the Pleistocene series/epoch of the quaternary system/period. Episodes, v. 44, pp. 241–247.

Head, M.J., Aubry, M.P., Piller, W.E., and Walker, M., 2023a. The Standard Auxiliary Boundary Stratotype: a replacement for the Auxiliary Stratotype Point in supporting a Global boundary Stratotype Section and Point (GSSP). Episodes, v. 46, pp. 35–45. doi:10.18814/epiiugs/2022/022012

Head, M.J., Aubry, M.P., Piller, W.E., and Walker, M., 2023b. Standard Auxiliary Boundary Stratotype (SABS) approved to support the Global boundary Stratotype Section and Point (GSSP). Episodes, v. 46, pp. 99–100. doi:10.18814/epiiugs/2022/022044

Head, M.J., Aubry, M.P., Piller, W.E., and Walker, M., 2022, The Standard Auxiliary Boundary Stratotype: a replacement for the Auxiliary Stratotype Point in supporting a Global boundary Stratotype Section and Point (GSSP). Episodes, online doi:10.18814/epiiugs/2022/022012

Horng, C. S., Lee, M. Y., Palike, H., Wei, K.Y., Liang, W. T., Iizuka, Y., and Torii, M., 2002, Astronomically calibrated ages for geomagnetic reversals within the Matuyama Chron. Earth Planets Space, v. 54, pp. 679–690.

Horng, C., Roberts, A. P., and Liang, W., 2003, A 2.14-Myr astronomically tuned record of relative geomagnetic paleointensity from the western Philippine Sea. Journal of Geophysical Research, v. 108(B1), 2059, doi:10.1029/2001JB001698

Izumi, K., Haneda, Y., Suganuma, Y., Okada, M., Kubota, Y., Nishida, N., Kawamata, M., and Matsuzaki, T., 2021, Multiproxy sedimentological and geochemical analyses across the Lower–Middle Pleistocene boundary: chemostratigraphy and paleoenvironment of the Chiba composite section, central Japan. Progress in Earth Planetary Science, v. 8, doi:10.1186/s40645-020-00393-5

Jicha, B.R., Singer, B.S., and Sobol, P., 2016, Re-evaluation of the ages of $^{40}Ar/^{39}Ar$ sanidine standards and supereruptions in the western U.S. using a Noblesse multicollector mass spectrometer. Chemical Geology, v. 431, pp. 54–66.

Joannin, S., Ciaranfi N., and Stefanelli, S., 2008, Vegetation changes during the late Early Pleistocene at Montalbano Jonico (Province of Matera, southern Italy) based on pollen analysis. Palaeogeography, Palaeoclimatology, Palaeoecology, v. 270, pp. 92–101.

Jouzel, J., Masson-Delmotte, V., Cattani, O., Dreyfus, G., Falourd, S., Hoffmann, G., Minster, B., Nouet, J., Barnola, J.M., Chappellaz, J., Fischer, H., Gallet, J.C., Johnsen, S., Leuenberger, M., Loulergue, L., Luethi, D., Oerter, H., Parrenin, F., Raisbeck, G., Raynaud, D., Schilt, A., Schwander, J., Selmo, E., Souchez, R., Spahni, R., Stauffer, B., Steffensen, J.P., Stenni, B., Stocker, T.F., Tison, J.L., Werner, M., and Wolff, E.W., 2007, Orbital and millennial Antarctic climate variability over the past 800,000 years. Science, v. 317, pp. 793–796.

Kameo, K., Kubota, Y., Haneda, Y., Suganuma, Y., and Okada, M., 2020, Calcareous nannofossil biostratigraphy of the Lower–Middle Pleistocene boundary of the GSSP, Chiba composite section in the Kokumoto

Formation, Kazusa Group, central Japan, and implications for sea-surface environmental changes. Progress in Earth and Planetary Science, v. 7, pp. 36, doi:10.1186/s40645-020-00355-x

Kazaoka, O., Suganuma, Y., Okada, M., Kameo, K., Head, M.J., Yoshida, T., Kameyama, S., Nirei, H., Aida, N., and Kumai, H., 2015, Stratigraphy of the Kazusa Group, Central Japan: a high-resolution marine sedimentary sequence from the Lower to Middle Pleistocene. Quaternary International, v. 383, pp. 116–135.

Kleiven, H., Hall, I.R., McCave, I.N., Knorr, G., and Jansen, E., 2011, North Atlantic coupled deep-water flow and climate variability in the middle Pleistocene. Geology, v. 39, pp. 343–346.

Köhler, P., Fischer, H., Munhoven, G., and Zeebe, R.E., 2005, Quantitative interpretation of atmospheric carbon records over the last glacial termination. Global Biogeochem. Cycles 19, doi:10.1029/2004GB002345.%20GB4020

Konijnendijk, T.Y.M., Ziegler, M., and Lourens, L.J., 2015, On the timing and forcing mechanisms of late Pleistocene glacial terminations: Insights from a new high-resolution benthic stable oxygen isotope record of the eastern Mediterranean. Quaternary Science Reviews, v. 129, pp. 308–320.

Kubota, Y., Haneda, Y., Kameo, K., Itaki, T., Hayashi, H., Shikoku K, Izumi, K., Head, M.J., Suganuma, Y., and Okada. M., 2021, Paleoceanography of the northwestern Pacific across the Early–Middle Pleistocene boundary (Marine Isotope Stages 20–18). Progress in Earth Planetary Sciences, v. 8, pp.1–24. doi:10.1186/s40645-020-00395-3

Langereis, C.G., Dekkers, M.J., de Lange., G.J., Paterne, M., and van Santvoort, P.J.M., 1997, Magnetostratigraphy and astronomical calibration of the last 1.1 Myr from an eastern Mediterranean piston core and dating of short events in the Brunhes. Geophysical Journal International, v. 129, pp. 75–94.

Laskar, J., Robutel, P., Joutel, F., Gastineau, M., Correia, A.C.M., and Levrard, B., 2004, A long termnumerical solution for the insolation quantities of the Earth. Astron. Astrophys, v. 428, pp. 261–285, doi:10.1051/0004-6361:20041335

Lionello, P., 2012. The climate of the Mediterranean region, from the past to the future. Elsevier, doi:10.1016/C2011-0-06210-5

Lionello, P., Malanotte-Rizzoli, P., and Boscolo, R., 2006, Mediterranean climate variability, Elsevier, ISBN: 0-444-52170-4, 438 pp.

Lirer, F., Caruso, A., Cosentino, C., Turco, E., Sierro, F., Salvatorini, G., Foresi, L., and Iaccarino, S., 2019, Mediterranean Neogene planktonic foraminifer biozonation and biochronology. Earth-Science Reviews, v. 196, doi:10.1016/j.earscirev.2019.05.013

Lisiecki, L.E., and Raymo, M.E., 2005, A Pliocene–Pleistocene stack of 57 globally distributed benthic $\delta^{18}O$ records. Paleoceanography, 20, PA1003.

Lisiecki, L. E., and Stern, J. V., 2016, Regional and global benthic $\delta^{18}O$ stacks for the last glacial cycle, Paleoceanography, v. 31, pp. 1–27, doi:10.1002/2016PA003002

Lourens, L.J., Hilgen, F.J., Raffi, I., and Vergnaud-Grazzini, C., 1996, Early Pleistocene chronology of the Vrica section (Calabria, Italy). Paleoceanography, v. 11, pp. 797–812.

Lourens, L.J., 2004, Revised tuning of Ocean Drilling Program Site 964 and KC01B (Mediterranean) and implications for the $\delta^{18}O$, tephra, calcareous nannofossil, and geomagnetic reversal chronologies of the past 1.1 Myr. Paleoceanography, 19, PA3010.

Lourens, L.J., Hilgen, F.J., and Raffi, I., 1998, Base of large Gephyrocapsa and astronomical calibration of early Pleistocene sapropels in Site 967 and Hole 969D: solving the chronology of the Vrica section (Calabria, Italy). In: Robertson, H.F., Emeis, K., Richter, C., et al. (Eds.), Proceedings of the Ocean Drilling Program: Scientific Results, v. 160, pp. 191–198. College Station, TX.

Lourens, L., Hilgen, F., Shackleton, N.J., Laskar, J., and Wilson, D., 2004, The Neogene period. In: Gradstein, F.M., Ogg, J.G., Smith, A.G. (Eds.), A Geological Time Scale. Cambridge University Press, pp. 409–440.

Macrì, P., Capraro, L., Ferretti, P., and Scarponi, D., 2018, A high-resolution record of the Matuyama–Brunhes transition from the Mediterranean region: The Valle di Manche section (Calabria, Southern Italy). Physics of the Earth and Planetary Interiors, v. 278, pp. 1–15.

Maiorano, P., Aiello, G., Barra, D., Di Leo, P., Joannin, S., Lirer, F., Marino, M., Pappalardo, A., Capotondi, L., Ciaranfi, N., and Stefanelli, S., 2008, Paleoenvironmental changes during sapropel 19 (i-cycle 90) deposition: evidences from geochemical, mineralogical and microplaoentological proxies in the mid Pleistocene Montalbano Jonico land section (southern Italy). Palaeogeography, Palaeoclimatology, Palaeoecology, v. 257, pp. 308–334.

Maiorano, P., Bertini, A., Capolongo, D., Eramo, G., Gallicchio, S., Girone, A., Pinto, D., Toti, F., Ventruti, G., and Marino, M., 2016, Climate signatures through the Marine Isotope Stage 19 in the Montalbano Jonico section (Southern Italy): a land-sea perspective. Palaeogeography, Palaeoclimatology, Palaeoecology, v. 461, pp. 341–361.

Maiorano, P., Capotondi, L., Ciaranfi, N., Girone, A., Lirer, F., Marino, M., Pelosi, N., Petrosino, P., and Piscitelli, A., 2010, Vrica-Crotone and Montalbano Jonico sections: a potential unit-stratotype of the Calabrian Stage. Episodes, v. 33, pp. 218–233.

Maiorano, P., and Marino, M., 2004. Calcareous nannofossil bioevents and environmental control on temporal and spatial pattern at the early–middle Pleistocene. Marine Micropaleontology, v. 53, pp. 405–422.

Maiorano, P., Marino, M., Di Stefano, E., and Ciaranfi, N., 2004. Calcareous nannofossil events in the lower–middle Pleistocene transition at the Montalbano Jonico section and ODP Site 964: calibration with isotope and sapropel stratigraphy. Rivista Italiana di Paleontologia e Stratigrafia, v. 110, pp. 547–557.

Maiorano, P., Marino, M., and De Lange, G. J., 2019, Dynamic surface-water alterations during sapropel S1 preserved in high-resolution shallow-water sediments of Taranto Gulf, central Mediterranean. Palaeogeography, Palaeoclimatology, Palaeoecology, v. 534, 109340. doi:10.1016/j.palaeo.2019.109340

Maiorano, P., Herbert, T.D., Marino, M., Bassinot, F., Bazzicalupo, P., Bertini, A., Girone, A., Nomade, S., and Ciaranfi, N., 2021, Paleoproductivity modes in central Mediterranean during MIS 20–MIS 18: calcareous plankton and alkenone variability. Paleoceanography Paleoclimatololgy, v. 36, e2021PA004259, doi:10.1029/2021PA004259

Mangili, C., Brauer, A., Plessen, B., and Moscariello, A. 2007, Centennial-scale oscillations in oxygen and carbon isotopes of endogenic calcite from a 15,500 varve year record of the Piànico interglacial. Quaternary Science Reviews, v. 26, pp. 1725–1735, doi:10.1016/j.quascirev.2007.04.012

Marino, M., 1996. Quantitative nannofossil biostratigraphy of the lower–middle Pleistocene Montalbano Jonico section, southern Italy. Paleopelagos, v. 6, pp. 347–360.

Marino, M., Aiello, G., Barra, D., Bertini, A., Gallicchio, S., Girone, A., La Perna, R., Lirer, F., Maiorano, P., Petrosino, P., Quivelli, O., Toti, F., and Ciaranfi, N., 2016, The Montalbano Jonico section (South Italy) as a reference for the Early/Middle Pleistocene boundary. Alpine and Mediterranean Quaternary, v. 29, n. 1, pp. 45–57.

Marino, M., Bertini, A., Ciaranfi, N., Aiello, G., Barra, D., Gallicchio, S., Girone, A., La Perna, R., Lirer, F., Maiorano, P., Petrosino, P., and Toti, F., 2015, Paleoenvironmental and climatostratigraphic insights for Marine Isotope Stage 19 (Pleistocene) at the Montalbano Jonico section, South Italy. Quaternary International, v. 383, pp.104–115, doi:10.1016/j.quaint.2015.01.043

Marino, M., Girone, A., Gallicchio, S., Herbert, T., Addante, M., Bazzicalupo, P., Quivelli, O., Bassinot, F., Bertini, A., Nomade, S., Ciaranfi, N., and Maiorano, P., 2020, Climate variability during MIS 20–18 as recorded by alkenone-SST and calcareous plankton in the Ionian Basin (central Mediterranean). Palaeogeography, Palaeoclimatology, Palaeoecology, v. 560, 110027.

Mark, D.F., Renne, P.R., Dymock, R.C., Smith, V.C., Simon, J.I., Morgan, L.E., Staff, R.A., Ellis, B.S., and Pearce, N.J., 2017, High-precision 40Ar/39Ar dating of Pleistocene tuffs and temporal anchoring of the Matuyama–Brunhes boundary. Quaternary Geochronology, v. 39, pp. 1–23, doi:10.1016/j.quageo.2017.01.002

Massari, F., Rio, D., Sgavetti, M., Prosser, G., D'Alessandro, A., Asioli, A., Capraro, L., Fornaciari, E., and Tateo, F., 2002, Interplay between tectonics and glacioeustasy, Pleistocene of the Crotone Basin, Calabria (southern Italy). Geological Society American Bullettin, v. 114, pp. 1183–1209.

Meyers, S.R., Siewert, S.E., Singer, B.S., Sageman, B.B., Condon, D.J., Obradovich, J.D., Jicha, B.R., and Sawyer, D.A., 2012, Intercalibration of radioisotopic and astrochonologic time scales for the Cenomanian-Turonian boundary interval, Western Interior Basin, USA. Geology, v. 40, pp. 7–10.

Milligan, T.G., and Cattaneo, A., 2007, Sediment Dynamics in the Western Adriatic Sea: From transport to stratigraphy. Continental Shelf Research, v. 27, pp. 287–295.

Min, K., Mundil, R., Renne, P.R., and Ludwig, K.R., 2000, A test for systematic errors in 0Ar/39Ar geochronology through comparison with U/Pb analysis of a 1.1-Ga rhyolite: Geochimica et Cosmochimica Acta, v. 64, pp. 73–98, doi:10.1016/S0016-7037(99)00204-5

Mix, A.C., Pisias, N.G., and Rugh, W., 1995a, Benthic foraminiferal stable isotope record from Site 849: 0–5 Ma, in Pisias, N.G., Mayer, L., Janecek, T., Palmer-Julson, A., and van Andel, T.H., eds., Proceedings of the Ocean Drilling Program: Scientific Results, v. 138, College Station (TX), pp. 371–412.

Mix, A.C., Le, J., and Shackleton, N.J., 1995b, Benthic foraminifer stable isotope stratigraphy of Site 846: 0–1.8 Ma, in Pisias, N.G., Mayer, L., Janecek, T., Palmer-Julson, A., and van Andel, T.H., eds., Proceedings of the Ocean Drilling Program: Scientific Results, v. 138, College Station (TX), pp. 839–856.

Moscariello, A., Ravazzi, C., Brauer, A., Mangili, C., Chiesa, S., Rossi, S., de Beaulieu, J.L., and Reille, M., 2000, A long lacustrine record from the Pianico-Sellere Basin (Middle–Late Pleistocene, Northern Italy). Quaternary International, v. 73/74, pp. 47–68.

Mostardini, F., and Pieri, P., 1967, Note illustrative della Carta Geologica d'Italia alla scala 1:100.000, Foglio 212 Montalbano Ionico. La Litografica, Roma.

Negri, A., Amorosi, A., Antonioli, F., Bertini, A., Florindo, F., Lurcock, P.C., Marabini, S., Mastronuzzi, G., Regattieri, E., Rossi, V., Scarponi, D., Taviani, M., Zanchetta, G., and Vai, G.B., 2015, A potential global boundary stratotype section and point (GSSP) for the Tarentian Stage, Upper Pleistocene, from the Taranto area (Italy): results and future perspectives. Quaternary International, v. 383, pp. 145–157. doi:10.1016/j.quaint.2014.08.057

Nishida N, Kazaoka O, Izumi K, Suganuma Y, Okada M, Yoshida T, Ogitsu I, Nakazato H, Kameyama, S., Kagawa, A., Morisaki, M., and Nirei, H., 2016, Sedimentary processes and depositional environments of a continuous marine succession across the Lower–Middle Pleistocene boundary: Kokumoto Formation, Kazusa Group, central Japan. Quaternary International, v. 397, pp. 3–15.

Nomade, S., Bassinot, F., Marino, M., Simon, Q., Dewilde, F., Maiorano, P., Isguder, G., Blamart, D., Girone, A., Scao, V., Pereira, A., Toti, F., Bertini, A., Combourieu-Nebout, N., Peral, M., Bourles, D.L., Petrosino, P., Gallicchio, S., and Ciaranfi, N., 2019, Highresolution foraminifer stable isotope record of MIS 19 at Montalbano Jonico, southern Italy: A window into Mediterranean climatic variability during a low-eccentricity interglacial. Quaternary Science Reviews, v. 205, pp.106–125.

Okada, M., and Suganuma, Y., 2018, Report on the PO-5 field trip to the GSSP candidate for the Middle Pleistocene Subseries on the Yoro River (Chiba Section, Japan), held during the XIX INQUA Congress 2015, 3–4 August 2015. Quaternary Perspectives, v. 25, pp. 22.

Okada, M., Suganuma, Y., Haneda, Y., and Kazaoka, O., 2017, Paleomagnetic direction and paleointensity variations during the Matuyama–Brunhes polarity transition from a marine succession in the Chiba composite section of the Boso Peninsula, central Japan. Earth, Planets, and Space, v. 69, p. 45, doi:10.1186/s40623-017-0627-1

Patacca, E., and Scandone, P., 2007, Geology of the Southern Apennines. Bolettino. Società Geologica Italiana, Special Issue 7, pp. 75–119.

Peral, M., Blamart, D., Bassinot, F., Daeron, M., Dewilde, F., Rebaubier, H., Nomade, S., Girone, A., Marino, M., Maiorano, P., and Ciaranfi, N., 2020, Changes in temperature and oxygen isotopic composition of Mediterranean water during the Mid-Pleistocene transition in the Montalbano Jonico section (southern Italy) using the clumped-isotope thermometer. Palaeogeography, Palaeoclimatologu, Palaeoecology 544, ISSN: 0031-0182, doi:10.1016/J.PALAEO.2020.109603

Petrosino, P., Jicha, B.R., Mazzeo, F.C., Ciaranfi, N., Girone, A., Maiorano, P., and Marino, M., 2015, The Montalbano Jonico marine succession: An archive for distal tephra layers at the Early–Middle Pleistocene boundary in southern Italy. Quaternary International, v. 383, pp. 89–103. doi:10.1016/j.quaint.2014.10.049

Pieri, P., Sabato, L., and Tropeano, M., 1996, Significato geodinamico dei caratteri deposizionali e strutturali della Fossa bradanica nel Pleistocene. Memorie Società Geologica Italiana, v. 51, pp. 501–515.

Pol, K., Masson-Delmotte, V., Johnsen, S., Bigler, M., Cattani, O., Durand, G., Falourd, S., Jouzel, J., Minster, B., Parrenin, F., Ritz, C., Steen-Larsen, H. C., and Stenni, B., 2010, New MIS 19 EPICA Dome C high resolution deuterium data: hints for a problematic preservation of climate variability in the "oldest ice". Earth and Planetary Science Letters. doi:10.1016/j.epsl.2010.07.030

Poulain, P.M., 2001, Adriatic Sea surface circulation as derived from drifter data between 1990 and 1999. Journal Marine Systems, v. 29, pp. 3–32.

Pujol, C., and Vergnaud-Grazzini, C., 1995, Distribution patterns of live planktic foraminifers as related to regional hydrography and productive systems of the Mediterranean Sea. Marine Micropaleontology, v. 25, pp.187–217.

Quivelli, O., Marino, M., Rodrigues, T., Girone, A., Maiorano, P., Bertini, A., Niccolini, G., Trotta, S., and Bassinot, F., 2021, Multiproxy record of suborbital-scale climate changes in the Algero-Balearic Basin during late MIS 20 - Termination IX. Quaternary Science Reviews, v. 260, 106916. doi:10.1016/j.quascirev.2021.106916

Raffi, I., 2002, Revision of the early–middle Pleistocene calcareous nannofossil biochronology (1.75–0.85 Ma). Marine Micropaleontology, v. 45, pp. 25–55.

Raffi, I., Agnini, C., Backman, J., and Catanzariti, R., 2016, A Cenozoic calcareous nannofossil biozonation from low and middle latitudes: A synthesis. Journal of Nannoplankton Research, v. 36, pp. 121–132.

Raffi, I., Backman, J., Fornaciari, E., Pälike, H., Rio, D., Lourens, L., and Hilgen, F., 2006, A review of calcareous nannofossil astrobiochronology encompassing the past 25 million years. Quaternary Science Reviews, v. 25, pp. 3113–3137.

Raisbeck, G.M., You, F., Cattani, O., and Jouzel, J., 2006, ^{10}Be evidence for the Matuyama–Brunhes geomagnetic reversal in the EPICA Dome C ice core. Nature, v. 444, pp. 82–84.

Regattieri, E., Giaccio, B., Mannella, G., Zanchetta, G., Nomade, S., Tognarelli, A., Perchiazzi, N., Vogel, H., Boschi, C., Neil, R.D., Wagner, B., Gemelli, M., and Tzedakis, P., 2019, Frequency and dynamics of millennial-scale variability during Marine Isotope Stage 19: Insights from the Sulmona Basin (central Italy). Quaternary Science Reviews, v. 214, pp. 28–43.

Richmond, G.M., 1996, The INQUA-approved provisional Lower–Middle Pleistocene boundary. In: Turner, C. (Ed), The early Middle Pleistocene in Europe. Balkema, Rotterdam, pp. 319–327.

Rio, D., Raffi, I., and Villa, G., 1990, Pliocene–Pleistocene distribution patterns in the Western Mediterranean. In: Karstetn, K.A., Mascle, J., et al. (Eds.), Proceedings of ODP, Scientific Results, v. 107, pp. 513–533.

Rio, D., Sprovieri, R., Castradori, D., and Di Stefano, E., 1998, The Gelasian Stage (Upper Pliocene): a new unit of the global standard chronostratigraphic scale. Episodes, v. 21, pp. 82–87.

Roberts, A. P., Florindo, F., Larrasoaña, J. C., O'Regan, M. A., and Zhao, X., 2010, Complex polarity pattern at the (former) Plio?Pleistocene

global stratotype section at Vrica (Italy): Remagnetization by magnetic iron sulphides. Earth Planetary Science Letters, v. 292, pp. 98–111, doi:10.1016/j.epsl.2010.01.025

Rohling, E., and Palike, H., 2005, Centennial-scale climate cooling with a sudden cold event around 8,200 years ago. Nature, v. 434, pp. 975–979.

Rohling, E.J., Jorissen, F.J., and De Stigter, H.C., 1997, 200 year interruption of Holocene sapropel formation in the Adriatic Sea. Journal of Micropalaeontology, v. 16, pp. 97–108.

Rohling, E.J., Marino, G., and Grant, K.M., 2015, Mediterranean climate and oceanography, and the periodic development of anoxic events (sapropels). Earth Science Reviews, v. 143, pp. 62–97.

Rodrigues, T., Alonso-Garcia, M., Hodell, D. A., Rufino, M., Naughton, F., Grimalt, J. O., Voelker, A.O., andAbrantes, F., 2017, A 1-Ma record of sea surface temperature and extreme cooling events in the North Atlantic: A perspective from the Iberian margin. Quaternary Science Reviews, v. 172, pp. 118–130. doi:10.1016/j.quascirev.2017.07.004

Rossi, S., 2003, Etude pollinique de la séequence lacustre Pléistocène de Piànico-Sèllere (Italie). Ph.D. Thesis. Universitè de Droit d'Economie et des Sciences d'Aix Marseille M. Marino, et al. Palaeogeography, Palaeoclimatology, Palaeoecology, v. 560, 110027III.

Sagnotti, L., Cascella, A., Ciaranfi, N., Macrì, P., Maiorano, P., Marino, M., and Taddeucci, J., 2010, Rock magnetism and paleomagnetism of the Montalbano Jonico section (Italy): evidence for late diagenetic growth of greigite and implications for magnetostratigraphy. Geophysical Journal International, v. 180, pp. 1049–1066.

Sagnotti, L., Giaccio, B., Liddicoat, J.C., Nomade, S., Renne, P.R., Scardia, G., and Sprain, C.J., 2016, How fast was the Matuyama–Brunhes geomagnetic reversal? A new subcentennial record from the Sulmona Basin, central Italy. Geophysical Journal Interiors, v. 204, pp. 798–812.

Sagnotti, L., Scardia, G., Giaccio, B., Liddicoat, J.C., Nomade, S., Renne, P.R., and Sprain, C.J., 2014. Extremely rapid directional change during Matuyama–Brunhes geomagnetic polarity reversal. Geophysical Journal International. doi:10.1093/gji/ggu287

Sánchez-Goñi, M.F., Rodrigues, T., Hodell, D.A., Polanco-Martínez, J.M., Alonso-García, M., Hernández-Almeida, I., Desprat, S., and Ferretti, P., 2016, Tropically-driven climate shifts in southwestern Europe during MIS 19, a low eccentricity interglacial. Earth Planetary Science Letters, v. 448, pp. 81–93.

Sangiorgi, F., Dinelli, E., Maffioli, P., Capotondi, L., Giunta, S., Morigi, C., Principato, M. S., Negri, A., Emeis, K.C., and Corselli, C. 2006, Geochemical and micropaleontological characterisation of a Mediterranean sapropel S5: A case study from core 20 BAN89GC09 (south of Crete). Palaeogeography, Palaeoclimatology, Palaeoecology, v. 235, pp. 192–207, doi:10.1016/j.palaeo.2005.09.029

Savini, A., and Corselli, C., 2010, High-resolution bathymetry and acoustic geophysical data from Santa Maria di Leuca Cold Water Coral province (Northern Ionian Sea-Apulian continental slope). Deep-Sea Research II, v. 57, pp. 326–344.

Sella, M., Turci, C., and Riva, A., 1988, Sintesi geopetrolifera della Fossa Bradanica (Avanfossa della catena Appenninica). Mem. Soc. Geol. It., v. 41, pp 87–107.

Sgarrella, F., and Moncharmont-Zei, M., 1993, Benthic Foraminifera of the Gulf of Naples (Italy): systematics and autecology. Bollettino della Società Paleontologica Italiana, v. 32, pp. 145–264.

Shackleton, N.J., Crowhurst, S., Hagelberg, T., Pisias, N.G., and Schneider, D.A., 1995, A new late Neogene time scale: application to Leg 138 sites, in Pisias, N.G., Mayer, L., Janecek, T., Palmer-Julson, A., and van Andel, T.H. (Eds.), Proceedings of the Ocean Drilling Program, Scientific Results, v. 138, pp. 73–101.

Siani, G., Sulpizio, R., Paterne, M., and Sbrana, A., 2004, Tephrostratigraphy study for the last 18,000 14C years in a deep-sea sediment sequence for the South Adriatic, Quaternary Science Reviews, v. 23, pp. 2485–2500.

Simon, Q., Bourlès, L.D., Bassinot, F., Nomade, S., Marino, M., Ciaranfi, N., Girone, A., Maiorano, P., Thouveny, N., Choya, S., Dewil, F., Scao, V., Isguder, G., Blamart, D., and ASTER Team. 2017, Authigenic $^{10}Be/^{9}Be$ ratio signature of the Matuyama–Brunhes boundary in the Montalbano Jonico marine succession. Earth and Planetary Science Letters, v. 460, pp. 255–267.

Simon, Q., Bourlès, D.L., Thouveny, N., Horng, C.H., Valet, J.P., Bassinot, F., and Choy, S., 2018, Cosmogenic signature of geomagnetic reversals and excursions from the Reunion event to the Matuyama–Brunhes transition (0.7–2.14 Ma interval). Earth Planetary Science Letters, v. 82, pp. 510–524.

Simon, Q., Suganuma, Y., Okada, M., Haneda, Y., and ASTER Team, 2019, High-resolution ^{10}Be and paleomagnetic recording of the last polarity reversal in the Chiba composite section: age and dynamics of the Matuyama–Brunhes transition Earth Planetary Science Letters, v. 519, pp. 92–100.

Simon, Q., Thouveny, N., Bourlès, D.L., Valet, J.P., Bassinot, F., Ménabréaz, L., Guillou, V., Choy, S., and Beaufort, L., 2016, Authigenic $^{10}Be/^{9}Be$ ratio signatures of the cosmogenic nuclide production linked to geomagnetic dipole moment variation since the Brunhes/Matuyama boundary. Journal Geophysical Research, Solid Earth 121. doi:10.1002/2016JB013335

Singer, B.S., 2014, A quaternary geomagnetic instability time scale. Quaternary Geochronology, v. 21, pp. 29–52.

Singer, B.S., Jicha, B.R., Mochizuki, N., and Coe, R.S., 2019, Synchronizing volcanic, sedimentary, and ice core records of Earth's last magnetic polarity reversal. Science Advances, v. 5, eaaw4621. doi:10.1126/sciadv.aaw4621. PMID: 31457087; PMCID: PMC6685714.

Smith, M.E., Carrol, A.R., and Singer, B.S., 2008, Synoptic reconstruction of a major ancient lake system: Eocene Green River Formation, western United States: Geological Society of America Bulletin, v. 120, pp. 54–84.

Stefanelli, S., 2003, Benthic foraminiferal assemblages as tools for paleoenvironmental reconstruction of the early–middle Pleistocene Montalbano Jonico composite section. Bollettino della Società Paleontologica Italiana, v. 42, p. 281–299.

Stefanelli, S., 2004, Cyclic stages in oxygenation based on foraminiferal microhabitats: early–middle Pleistocene, Lucania basin, southern Italy. Journal of Micropaleontology, v. 23, pp. 81–95.

Stefanelli S., Capotondi, L., and Ciaranfi, N., 2005, Foraminiferal record and environmental changes during the deposition of early–middle Pleistocene sapropels in southern Italy. Palaeogeography, Palaeoclimatology, Palaeoecology, v. 216, pp. 27–52.

Suc J.P., Combourieu-Nebout, N., Seret,G., Popescu, S.A., Klotz, S., Gautier, F., Clauzon, G., Westgate, J., Insinga, D., and Sandhu, A.S., 2010, The Crotone series: a synthesis and new data. Quaternary International, v. 219, pp. 121–133.

Suganuma, Y., Okada, M., Horie, K., Kaiden, H., Takehara, M., Senda, R., Kimura, J.I., Kawamura, K., Haneda, Y., Kazaoka, O., and Head, M.J., 2015, Age of Matuyama–Brunhes boundary constrained by U–Pb zircon dating of a widespread tephra. Geology, v. 43, pp. 491–494, doi:10.1130/G36625.1

Suganuma, Y., Okuno, J., Heslop, D., Roberts, A.P., Yamazaki, T., and Yokoyama, Y., 2011, Post-depositional remanent magnetization lock-in for marine sediments deduced from ^{10}Be and paleomagnetic records through the Matuyama–Brunhes boundary. Earth and Planetary Science Letters, v. 311, pp. 39–52, doi:10.1016/j.epsl.2011.08.038

Suganuma, Y., Yokoyama, Y., Yamazaki, T., Kawamura, K., Horng, C.?S., and Matsuzaki, H., 2010, ^{10}Be evidence for delayed acquisition of remanent magnetization in marine sediments: Implications for a new age for the Matuyama-Brunhes boundary. Earth and Planetary Science Letters, v. 296, pp. 443–450, doi:j.epsl.2010.05.031

Suganuma, Y., Haneda, Y., Kameo, K., Kubota, Y., Hayashi, H., Itaki, T., Okuda, M., Head, M.J., Sugaya, M., Nakazato, H., Igarashi, A., Shikoku, K., Hongo, M., Watanabe, M., Satoguchi, Y., Takeshita, Y., Nishida, N., Izumi, K., Kawamura, K., Kawamata, M., Okuno, J., Yoshida, T., Ogitsu, I., Yabusaki, H., and Okada, M., 2018, Paleoclimatic and pale-

oceanographic records of Marine Isotope Stage 19 at the Chiba composite section, central Japan: A reference for the Early–Middle Pleistocene boundary. Quaternary Science Reviews, v. 191, pp. 406–430.

Suganuma, Y., Okada, M., Head, M.J., Kameo, K., Haneda, Y., Hayashi, H., Irizuki, T., Itaki, T., Izumi, K., Kubota, Y., Nakazato, H., Nishida, N., Okuda, M., Satoguchi, Y., Simon, Q., Takeshita, Y., and the Chiba composite section community members, 2021, Formal ratification of the Global Boundary Stratotype Section and Point (GSSP) for the Chibanian Stage and Middle Pleistocene Subseries of the Quaternary System: the Chiba Section, Japan. Episodes, doi:10.18814/epiiugs/2020/020080

Takeshita, Y., Matsushima, N., Teradaira, H., Uchiyama, T., and Kumai, H., 2016, A marker tephra bed close to the Middle Pleistocene boundary: Distribution of the Ontake-Byakubi tephra in central Japan. Quaternary International, v. 397, pp. 27–38, doi:10.1016/j.quaint.2015.03.054

Taricco, C., Vivaldo, G., Alessio, S., Rubinetti, S., and Mancuso, S., 2015, A high-resolution $\delta^{18}O$ record and Mediterranean climate variability. Climate of the Past, v. 11, pp. 509–522, doi:10.5194/cp-11-509-2015

Tauxe, L., Herbert, T., Shackleton, N.J., and Kok, Y.S., 1996, Astronomical calibration of the Matuyama–Brunhes boundary: consequences for magnetic remanence acquisition in marine carbonates and the Asian loess sequences. Earth Planetary Science Letters, v. 140, pp. 133–146.

Tesi, T., Asioli, A., Minisini, D., Maselli, V., Dalla Valle, G., Gamberi, F., Langone, L., Cattaneo, A., Montagna, P., and Trincardi, F., 2017, Large-scale response of the Eastern Mediterranean thermohaline circulation to African monsoon intensification during sapropel S1 formation. Quaternary Science Reviews, v. 159, pp. 139–154.

Toti, F., 2015, Interglacial vegetation patterns at the Early–Middle Pleistocene transition: a point of view from Montalbano Jonico section (southern Italy). Alpine and Mediterranean Quaternary, v. 28, pp. 131–143.

Tropeano, M., Cilumbriello, A., Sabato, L., Gallicchio, S., Grippa, A., Longhitano, S. G., Bianca, M., Gallipoli, M. R., Mucciarelli, M., and Spilotro, G., 2013, Surface and subsurface of the Metaponto Coastal Plain (Gulf of Taranto, southern Italy): Present-day vs LGM-landscape. Geomorphology, v. 203, pp. 115–131.

Turchetto, M., Boldrin, A., Langone, L., Miserocchi, S., Tesi, T., and Foglini, F., 2007, Particle transport in the Bari Canyon (southern Adriatic Sea). Marine Geology, v. 246, pp. 231–247.

Tzedakis, P.C., Channell, J.E.T., Hodell, D.A., Kleiven, H.F., and Skinner, L.C., 2012, Determining the natural length of the current interglacial. Nature Geoscience, v. 5, doi:10.1038/NGEO1358.

Valet, J.P., Bassinot, F., Bouilloux, A., Bourlès, D.L., Nomade, S., Guillou, V., Lopes, F., Thouveny, N., and Dewilde, F., 2014, Geomagnetic, cosmogenic and climatic changes across the last geomagnetic reversal from Equatorial Indian Ocean sediments. Earth Planetary Science Letters, v. 397, pp. 67–79, doi:10.1016/j.epsl.2014.03.053

Valet, J.P., Fand ournier, A., 2016, Deciphering records of geomagnetic reversals. Reviews of Geophysics, v. 54 pp. 410–446, doi:10.1002/2015RG000506

Valet, J.P., Fournier, A., Courtillot, V., and Herrero-Bervera, E., 2012, Dynamical similarity of geomagnetic field reversals. Nature, v. 490, pp. 89–94, doi:10.1038/nature11491

Valet, J.P., Meynadier, L., Simon, Q., and Thouveny, N., 2016, When and why sediments fail to record the geomagnetic field during polarity reversals? Earth Planetary Science Letters, v. 453, pp. 96–107.

Vannacci, M., 2016, Cambiamenti climatici durante lo stadio isotopico 22 come registrato nella successione marina di Montalbano Jonico (Italia meridionale) tramite indagine palinologica. Unpublished Master thesis. Università di Firenze, AA 2014–2015, p. 70.

Wagner, B., Vogel, H., and Francke, A., 2019, Mediterranean winter rainfall in phase with African monsoons during the past 1.36 million years. Nature, v. 573, pp. 256–260, doi:10.1038/s41586-019-1529-0

Walker, M., Head, M.J., Berkelhammer, M., Björck, S., Cheng, H., Cwynar, L., Fisher, D., Gkinis, V., Long, A., Lowe, J., Newnham, R., Rasmussen, S.O., and Weiss, H., 2018, Formal ratification of the subdivision of the Holocene series/Epoch (Quaternary system/period): two new Global Boundary Stratotype Sections and Points (GSSPs) and three new stages/subseries. Episodes Journal of International Geoscience, v. 41, pp. 213–223, doi:10.18814/epiiugs/2018/018016

Westaway, R., and Bridgland, D., 2009, Reply to comment by Riccardo Caputo and Marcello Bianca on 'Late Cenozoic uplift of southern Italy deduced from fluvial and marine sediments: Coupling between surface processes and lower-crustal flow' by Rob Westaway and David Bridgland; improved uplift modelling of the Gulf of Taranto marine terraces. Quaternary International, v. 210, pp. 102–109, doi:10.1016/j.quaint.2009.09.012

Wisshak, M., López Correa, M., Gofas, S., Salas, C., Taviani, M., Jakobsen, J., and Freiwald, A., 2009, Shell architecture, element composition, and stable isotope signature of the giant deep-sea oyster Neopycnodonte zibrowii sp. n. from the NE Atlantic. Deep-Sea Research I, v. 56, pp. 374–407.

Wright A.K., and Flower, B.P., 2002, Surface and deep ocean circulation in subpolar North Atlantic during the mid-Pleistocene revolution. Paleoceanography, v. 17, 1068, doi:1029/2002PA000782

Yin, Q., and Berger, A., 2015, Interglacial analogues of the Holocene and its natural near future. Quaternary Science Reviews, v. 120, pp. 28–46.

Maria Marino is specialist in micropaleontology and Associate Professor in Paleontology and Paleoecology at the Department of Earth and Geoenvironmental Sciences (University of Bari Aldo Moro, Italy). She mainly works on Quaternary stratigraphy and paleoclimate.

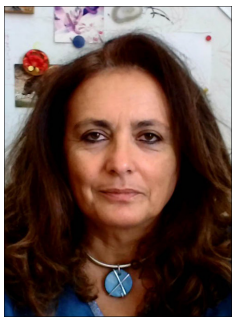

Angela Girone is Associate Professor in Paleontology and Paleoecology at the Department of Earth and Geoenvironmental Sciences (University of Bari Aldo Moro, Italy). Her researches focus on paleoclimate and paleobiogeography in Mediterranean and oceanic areas during Plio-Pleistocene.

Patrizia Maiorano is Associate Professor in Paleontology and Paleoecology at the Department of Earth and Geoenvironmental Sciences of the University of Bari, Italy and is a calcareous nannofossil specialist. Her main research interests concern Quaternary biostratigraphy and paleoclimate in Mediterranean and extra-Mediterranean marine deposits.

Salvatore Gallicchio, Ph.D in Earth Sciences, is Associate Professor at the Department of Earth and Geoenvironmental Sciences, University of Bari Aldo Moro, Italy. Skills and expertise: stratigraphy and facies analysis of Mesozoic to Tertiary successions of the Apennines; Geological field mapping.